

Eigenpatterns in southern California seismicity

K. F. Tiampo, J. B. Rundle,¹ S. McGinnis, and S. J. Gross

Cooperative Institute for Research in Environmental Sciences, University of Colorado, Boulder, Colorado, USA

W. Klein

Department of Physics, Boston University, Boston, Massachusetts, USA

Received 16 April 2001; revised 22 February 2002; accepted 21 May 2002; published 18 December 2002.

[1] Earthquakes in seismically active regions of the world are known to be associated with a variety of spatial and temporal patterns. Examples include precursory quiescence or activation, seismic clustering, and Mogi donuts. Although the characteristics of these patterns can be qualitatively described, a systematic quantitative analysis has proved elusive. In this paper we employ a new method, developed using numerical simulations, that allows a systematic quantification of the spatial and temporal characteristics of the patterns in historic seismicity in southern California. This method decomposes a set of boolean activity functions, representing historic seismicity, into their orthonormal eigenvalues and eigenfunctions. Here we show the results of this analysis which strongly support the hypothesis that seismic activity is highly correlated across many space scales and timescales within large volumes of the Earth's crust. *INDEX TERMS:* 7209 Seismology: Earthquake dynamics and mechanics; 7230 Seismology: Seismicity and seismotectonics; 3220 Mathematical Geophysics: Nonlinear dynamics; 7223 Seismology: Seismic hazard assessment and prediction; *KEYWORDS:* seismicity, fault system dynamics, southern California, mathematical methods in geophysics

Citation: Tiampo, K. F., J. B. Rundle, S. McGinnis, S. J. Gross, and W. Klein, Eigenpatterns in southern California seismicity, *J. Geophys. Res.*, 107(B12), 2354, doi:10.1029/2001JB000562, 2002.

1. Introduction

[2] Despite the relatively incomplete earthquake record, it has long been recognized that earthquake main shocks occur at quasiperiodic intervals and that, for some parts of the world, average recurrence intervals are well defined [Kanamori, 1981]. Both temporal and spatial clustering is evident in the data, with the result that neither the recurrent nature of the main shocks nor the observed phenomena such as foreshocks, aftershocks, seismic gaps, or main shock triggering are compatible with a Poisson probability function [Kagan and Jackson, 1992; Savage, 1993; Dieterich, 1994; Grant and Sieh, 1994; Rundle and Klein, 1995; Jones and Hauksson, 1997; Turcotte, 1997]. Much of the recent geological research associated with earthquakes has centered on investigating these spatial and temporal patterns in local and regional seismicity data [Kanamori, 1981]. Examples include, but are not limited to, characteristic earthquakes [Swan et al., 1980; Ellsworth and Cole, 1997], repeating earthquakes [Bakun et al., 1986; Marone et al., 1995], seismic gaps [Haberman, 1981; House et al., 1981; Kagan and Jackson, 1992; Wyss and Wiemer, 1999], well-defined recurrence intervals [Bakun and McEvilly, 1984; Lyzenga et al., 1991; Savage, 1993], Mogi donuts [Mogi, 1969],

temporal clustering [Frohlich, 1987; Press and Allen, 1995; Dodge et al., 1996; Eneva and Ben-Zion, 1997; Jones and Hauksson, 1997; Rundle et al., 1997; Huang et al., 1998], "slow" earthquakes [Linde et al., 1996; McGuire et al., 1996; Kerr, 1998], precursory quiescence [Yamashita and Knopoff, 1989; Wyss et al., 1996; Kato et al., 1997; Wyss et al., 2000], aftershock sequences [Gross and Kisslinger, 1994; Nanko et al., 1998], earthquake triggering over large distances [Stein et al., 1992; Hill et al., 1993; King et al., 1994; Hill et al., 1995; Deng and Sykes, 1996; Gomberg, 1996; Stark and Davis, 1996; Pollitz and Sacks, 1997; Stein, 1999], scaling relations [Rundle, 1989; Pacheco et al., 1992; Romanowicz and Rundle, 1993; Rundle, 1993; Saleur et al., 1995; Rundle et al., 1999], and time-to-failure analyses [Bufo and Varnes, 1993; Bowman et al., 1998; Gross and Rundle, 1998; Brehm and Braile, 1999; Jaume and Sykes, 1999]. Although this work represents important attempts to describe these characteristic patterns using empirical probability density functions, none of these observations or methodologies systematically identifies all possible seismicity patterns. The quantification of all possible space-time patterns would seem to be a necessary first step in the process of identifying which patterns are precursory to large events, leading to the possible development of new approaches in forecast methodology. Yet, as can be seen in Figure 1, a plot of relative southern California seismicity during the time period 1932–1991, the identification and quantification of these patterns is no easy matter.

¹Now at Center for Computational Science and Engineering, University of California, Davis, California, USA.

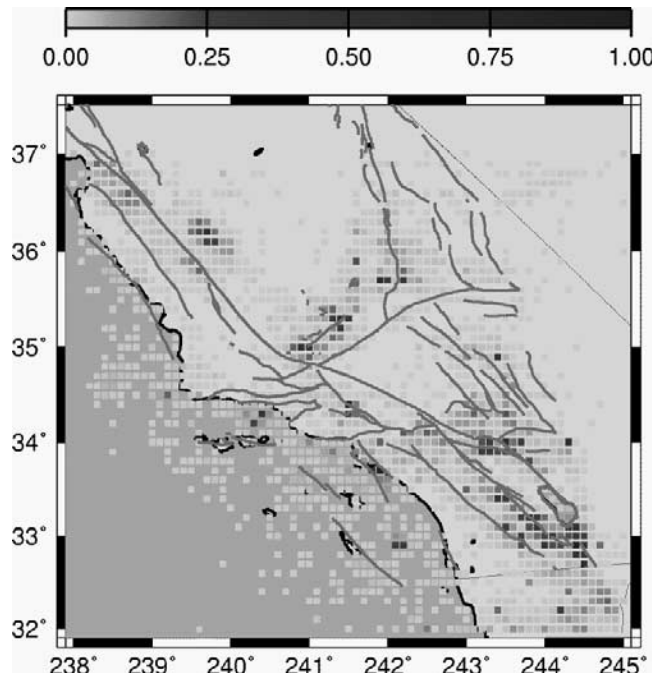


Figure 1. Seismicity for southern California, 1932–1991, normalized to the maximum number of events for the period.

[3] Earthquake fault systems are now thought to be an example of a complex nonlinear system [Bak *et al.*, 1987; Rundle and Klein, 1995]. Interactions among a spatial network of fault segments are mediated by means of a potential that allows stresses to be redistributed to other segments following slip on any particular segment. For faults embedded in a linear elastic host, this potential is a stress Green's function whose exact form can be calculated from the equations of linear elasticity, once the current geometry of the fault system is specified. A persistent driving force, arising from plate tectonic motions, increases stress on the fault segments. Once the stresses reach a threshold characterizing the limit of stability of the fault, a sudden slip event results. The slipping segment can also trigger slip at other locations on the fault surface whose stress levels are near the failure threshold as the event begins. In this manner, earthquakes occur that result from the interactions and nonlinear nature of the stress thresholds.

[4] Karhunen-Loeve methods, a linear decomposition technique in which a dynamical system is decomposed into a complete set of orthonormal subspaces, have been applied to a number of other complex nonlinear systems over the last fifty years, including the ocean-atmosphere interface, turbulence, meteorology, biometrics, statistics, and even geophysics [Hotelling, 1933; Fukunaga, 1970; Aubrey and Emery, 1983; Preisendorfer, 1988; Savage, 1988; Penland, 1989; Vautard and Ghil, 1989; Garcia and Penland, 1991; Penland and Magorian, 1993; Penland and Sardeshmukh, 1995; Holmes *et al.*, 1996; Moghaddam *et al.*, 1998]. In one such application, Savage [1988] decomposed the deformation at Long Valley caldera into its predominant modes in order to study only the signal that accounted for the greatest percentage of the variance, the volcanic source below the dome. In addition, he identified the primary error sources in the data using the remaining eigenmodes. In

another application, this technique was used to forecast the El Niño 3 sea surface temperatures [Penland, 1989; Vautard and Ghil, 1989; Penland and Magorian, 1993; Penland and Sardeshmukh, 1995].

[5] The notable success of this method in analyzing the ocean-atmosphere interface and such features as the El Niño-Southern Oscillation (ENSO), a nonlinear system whose underlying physics is governed by the Navier-Stokes equation, suggested its application to the analysis of the earthquake fault system [North, 1984; Preisendorfer, 1988; Penland and Magorian, 1993; Penland and Sardeshmukh, 1995]. Building on these methods for analyzing nonlinear threshold systems, space-time seismicity patterns can be identified in both numerical simulations using realistic earthquake models for southern California and actual historic seismicity records [Bufo and Varnes, 1993; Bowman *et al.*, 1998; Gross and Rundle, 1998; Brehm and Braile, 1999; Jaume and Sykes, 1999; Tiampo *et al.*, 1999; Rundle *et al.*, 2000; Tiampo *et al.*, 2000].

[6] In this paper, we apply this Karhunen-Loeve expansion (KLE) technique [Fukunaga, 1970; Holmes *et al.*, 1996] to the analysis of observed seismicity data from southern California in order to identify basis patterns for all possible space-time seismicity configurations. These basis states represent a complete, orthonormal set of eigenvectors and associated eigenvalues, obtained from the diagonalization of the correlation operators computed for the regional historic seismicity data translated into a set of boolean activity patterns over a given area. As a complete orthonormal basis set and a quantitative measure of the correlations in the seismicity data, these eigenvectors can be used for a variety of purposes, including, for example, formulation of a set of predictive Green's functions, or to reconstitute the data for various subset time periods of the entire data set [Fukunaga, 1970; Penland, 1989; Vautard and Ghil, 1989; Garcia and Penland, 1991; Penland and Magorian, 1993; Penland and Sardeshmukh, 1995; Holmes *et al.*, 1996; Moghaddam *et al.*, 1998].

2. Method

[7] Pattern evolution and prediction in nonlinear systems is complicated by nonlinear mode coupling and noise, but understanding such patterns, which are the surface expression of the underlying dynamics, is critical to understanding and perhaps characterizing the physics which control the system. Karhunen-Loeve expansion methods can be used to define a unique, complete pattern basis set for a given dynamical system [Fukunaga, 1970; North, 1984; Penland, 1989; Holmes *et al.*, 1996]. For driven threshold systems, an adaptation of these KLE methods can be employed to characterize both the space-time patterns of threshold transitions, i.e., “firings”, as well as the underlying, usually unobservable Markov variables that define the dynamics [Fukunaga, 1970; Holmes *et al.*, 1996; Rundle *et al.*, 2000]. In either case, the patterns are defined by the eigenstates and eigenvalues of one of an appropriately constructed family of correlation operators.

[8] Earthquake fault systems are examples of driven nonlinear threshold systems, comprised of interacting spatial networks of statistically identical, nonlinear units that are subjected to a persistent driving force [Scholz, 1990;

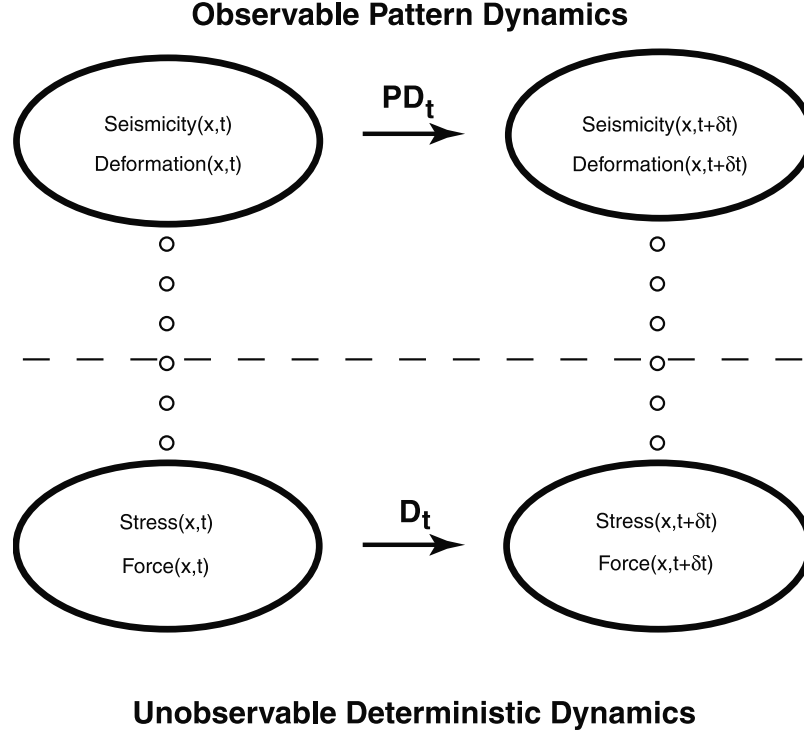


Figure 2. Schematic diagram of an earthquake threshold system.

[9] Rundle and Klein, 1995; Fisher et al., 1997; Rundle et al., 1997; Ferguson et al., 1999]. Numerous examples of such systems exist [Bak et al., 1987; Hertz et al., 1990; Herz and Hopfield, 1995; Fisher et al., 1997], of which earthquakes are but another example. Such systems are composed of cells which fire, or fail, when the driving force causes the force or potential, $\sigma(x, t)$ on a cell at location x and time t to reach a predefined threshold value σ^F . The behavior of these systems is determined by parameters such as threshold values, residual stresses, quenched disorder and noise [Bak et al., 1987; Rundle and Klein, 1995; Fisher et al., 1997]. Complex spatial and temporal firing patterns result which are difficult to analyze deterministically [Ouchi, 1993; Nijhout, 1997]. In the case of an earthquake fault system, the driving force is tectonic plate motion, and the internal potential is the stress on each fault cell or patch. The firing, or failure of each patch results in a decrease in the cell potential to some residual value σ^R . The interactions between the cells, or fault patches, may be excitatory, bringing another closer to failure, or inhibitory, in which the failure of one cell can move neighboring cells further from failure. The spatial and temporal firing patterns, i.e., the seismicity, of these driven threshold systems are complex and often difficult to understand and interpret from a deterministic perspective, as these patterns are emergent processes that develop from the obscure underlying structures, parameters, and dynamics of a multidimensional nonlinear system [Ouchi, 1993; Nijhout, 1997].

[10] Analysis of a number of these driven threshold systems often is complicated by the fact that the underlying dynamics and the state variables which control the physics of the system are unknown and difficult to observe. The earthquake fault system is no exception. While it is not only

probable, but essential, that space-time patterns and correlations exist in the variables and interactions which control earthquake dynamics, from which the observable surface patterns and correlations arise, those patterns are difficult or impossible to observe within the Earth [Scholz, 1990; Turcotte, 1997].

[11] The schematic shown in Figure 2 illustrates the physical problem. As the force at a particular location x evolves in time under the deterministic dynamics D_t , the stress, or potential, evolves in time as well. While the values of force and strain, along with the specifics of D_t , are hidden from view below the dashed line of Figure 2, the changes in surface deformation and seismicity are observable. In the earth, there is no means at present to measure the stress and strain at every point in an earthquake fault system, or the constitutive parameters which characterize the heterogeneous medium and its dynamics. However, the seismicity which is the surface expression of its firing activity can be located in both space and time with considerable accuracy [Bakun and McEvilly, 1984; Sieh et al., 1989; Hill et al., 1990] and can, for example, be characterized by a boolean time series. In this case, the firing activity, $\psi(x, t)$, can be represented as a set of time series at all positions x , where $\psi(x, t) = 1$ if an event occurs in the time interval between t and $t + \Delta t$, and $\psi(x, t) = 0$ otherwise.

[12] Two important points should be noted here. The first is that in this particular formulation, there is no specific information about creep events, which have no expression in the seismic history. Second, that there are other possible formulations of the activity function that might provide different or additional information about the seismicity. For example, time series might be formulated in which the value for each time bin is the summation of the total number of

events that occur in each time bin. Or, the total seismic moment, analogous to the seismic energy of these events could be used as the value at each time step. While we have tested several of these different constructions, the results are preliminary and outside the scope of this paper.

[12] *Rundle et al.* [2000] extended the standard KLE methods to include the construction of pattern states that can be used to forecast events in time, in much the same manner as EOF analysis is used to predict El Niño events in meteorology [*Preisendorfer*, 1988; *Penland*, 1989; *Garcia and Penland*, 1991]. This procedure involves constructing a correlation operator, $C(x_i, x_j)$, for the sites that contains the spatial relationship of slip events over time. $C(x_i, x_j)$ is decomposed into the orthonormal spatial eigenmodes for the nonlinear threshold system, e_j , and their associated time series, $a_j(t)$. In addition, *Rundle et al.* [2000] detailed the application of both an equal and an unequal time correlation operator on numerical simulations that extend over thousands of years. While an equal time correlation operator defines the existing correlations in the system, an unequal time correlation operator can be used to project the activity in question into the future, for forecasting purposes [*Ouchi*, 1993; *Penland*, 1989; *Nijhout*, 1997]. Although the development of unequal time correlation operator for actual data is theoretically possible, the choice of both the appropriate time step, time delay, and time period are not transparent. Finally, it is probable that the 60-year time period of available seismicity data in this region may not be long enough to ensure stationarity and a complete set of eigenvectors, the implication of which is still unknown. As a result, at this time we employ only an equal time correlation operator for our initial analysis and leave the development and study of forecasting operators for future work.

[13] The Karhunen-Loeve expansion is obtained from the p time series that record the deformation history at particular locations in space, where each time series consists of n time steps, $i = 1, \dots, n$, $y(x_s, t_i) = y_i^s$, and $s = 1, \dots, p$. The goal is to construct a time series for each of a large number of locations that records, for a given short period of time, whether an earthquake occurred at that location (value = 1) or did not occur (value = 0). If, for example, the time interval was decimated into units of 0.001 years, approximately eight hour time segments, the result would be a time series of 1000 time steps for every year of data, with either a zero or a one at each time step. These time series, or boolean activity functions, are incorporated into a matrix, T , consisting of time series of the same measurement for p different locations, i.e.,

$$T = [\bar{y}_1, \bar{y}_2, \dots, \bar{y}_p] = \begin{bmatrix} y_1^1 & y_1^2 & \dots & y_1^p \\ y_2^1 & y_2^2 & \dots & y_2^p \\ \vdots & \vdots & \dots & \vdots \\ y_n^1 & y_n^2 & \dots & y_n^p \end{bmatrix}.$$

T is therefore an $n \times p$ matrix of real values [*Fukunaga*, 1970].

[14] The covariance matrix, $S(x_i, x_j)$, for these events is formed by multiplying T by T^T , where S is a $p \times p$ real, symmetric matrix. The covariance matrix, $S(x_i, x_j)$, is converted to a correlation operator, $C(x_i, x_j)$, by dividing

each element of $S(x_i, x_j)$ by the variance of each time series, $y(x_i, t)$ and $y(x_j, t)$, as follows:

$$\sigma_p = \sqrt{\frac{1}{n} \sum_{k=1}^n (y_k^p)^2},$$

$$C = \begin{bmatrix} \frac{s_{11}}{\sigma_1 \sigma_1} & \frac{s_{12}}{\sigma_1 \sigma_2} & \dots & \frac{s_{1p}}{\sigma_1 \sigma_p} \\ \frac{s_{21}}{\sigma_2 \sigma_1} & \frac{s_{22}}{\sigma_2 \sigma_2} & \dots & \frac{s_{2p}}{\sigma_2 \sigma_p} \\ \vdots & \vdots & \dots & \vdots \\ \frac{s_{p1}}{\sigma_p \sigma_1} & \frac{s_{p2}}{\sigma_p \sigma_2} & \dots & \frac{s_{pp}}{\sigma_p \sigma_p} \end{bmatrix}$$

[15] This equal-time correlation operator, $C(x_i, x_j)$, is decomposed into its eigenvalues and eigenvectors in two parts. The first employs the trireduction technique to reduce the matrix C to a symmetric tridiagonal matrix, using a Householder reduction. The second part employs a ql algorithm to find the eigenvalues, λ_j^2 , and eigenvectors, e_j of the tridiagonal matrix [*Press et al.*, 1992]. These eigenstates thus represent the orthonormal basis vectors arranged in order of decreasing correlation, and reflect the relative importance of the various modes over the time interval of interest. Dividing the corresponding eigenvalues, λ_j^2 , by the sum of the eigenvalues, yields that percent of the correlation accounted for by that particular mode. The associated orthonormal time series can be reconstructed by projecting the initial data set onto these basis vectors [*Preisendorfer*, 1988; *Holmes et al.*, 1996]. The time-dependent expansion coefficients, $a_j(t)$, which represent temporal eigenvectors, are reconstructed by multiplying the original data matrix by the eigenvectors, i.e.,

$$a_j(t_i) = \bar{e}^T \cdot T = \sum_{s=1}^p e_j y_i^s,$$

where $j, s = 1, \dots, p$ and $i = 1, \dots, n$.

[16] This eigenstate decomposition technique produces the orthonormal spatial eigenmodes for this nonlinear threshold system, e_j , and the associated principal component time series, $a_j(t)$. These principal component time series represent the signal associated with each particular eigenmode over time. For purposes of clarity, the spatial eigenvectors are designated “KLE modes” and the associated time series “principal component (PC)” vectors.

3. Data

[17] The primary seismicity data set for southern California employed in this analysis is the entire California Institute of Technology catalog from 1932 through August 1999, obtained from the Southern California Earthquake Center (SCEC) database, with all blast events specifically removed from the catalog (available at <http://www.scec.org>). Relevant data include location, in latitude and longitude, and the time the event occurred. Seismic events between -115° and -122° longitude and 32° and 37° latitude were selected, and events of all quality were acquired. This particular area was chosen because it covers an area of the California fault system that is considered to be spatially interrelated and within which temporal correlations have been detected in the past [*Kanamori*, 1981; *Bufe and*

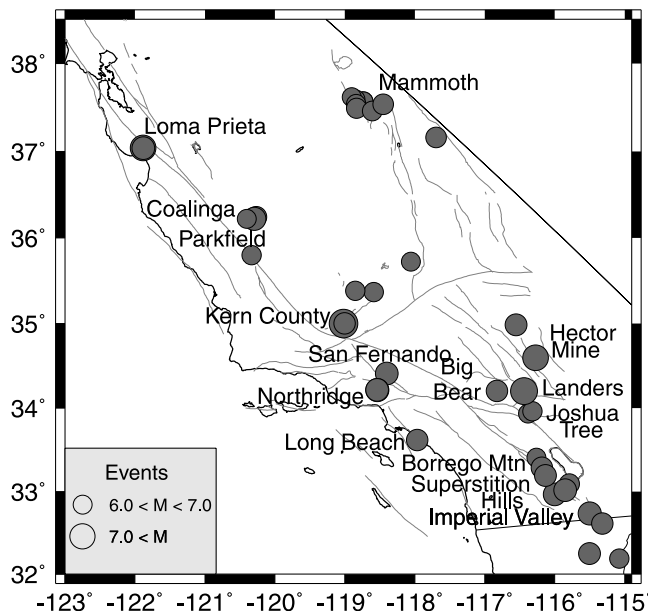


Figure 3. Location of major earthquakes in southern California, 1932–1999, as discussed in the text (www.scec.org). Included are a series of events associated with Mammoth Mountain eastern California that occurred throughout the 1980s.

Varnes, 1993; Press and Allen, 1995; Stark and Davis, 1996; Bowman *et al.*, 1998; Gross and Rundle, 1998; Brehm and Braile, 1999; Jaume and Sykes, 1999; Stein, 1999; Wyss *et al.*, 2000]. In addition, as the correlated regions around major past events are expected to be on the order of several hundred kilometers [Bowman *et al.*, 1998; Zoller *et al.*, 2001], this region was chosen to be several times larger than that, in order to encompass as many of the potential correlations as possible. Additional work, not detailed here, shows that while this region is large enough to reveal important features in the resulting eigenpatterns, it suggests, in addition, that applying this technique to variable region sizes may reveal important information on both the range of correlation and the interactions between major events in the catalog.

[18] Separate analyses were performed for the entire data set, consisting of all events of magnitude greater than or equal to 0.0, and on another data set in which only those events of magnitude greater than or equal to 3.0 were included in the binning process described below. While we recognize that the seismic network in southern California has changed significantly in regards to location, quality, and completeness, particularly at the low magnitude end, analysis of a catalog with no magnitude cut allows for the study of both the spatial and temporal completeness of the catalog and the network, as will be seen below. One of the most common uses of this technique in other fields is the removal of undesirable modes, such as noise or uninteresting secular signals, so that certain modes can be studied in more detail. The recognition, quantification, and removal of the detectability mode, both spatially and temporally, is one of the goals of this research, and will hopefully, in the future, eliminate the need for the application of a relatively arbitrary magnitude cutoff.

[19] The time periods evaluated were from 1932 to 1991, and 1932 through August 1999. In both cases, the seismicity was binned into squares of 0.1° latitude and 0.1° longitude to a side, and a time series constructed for each location square, boxes of approximately 11 km to a side, although this varies slightly over the 5° of latitude. Each time step is given an initial value of 1.0 if one or more events occurs in that time period, or a value of 0.0 otherwise. Subsequently, the mean for each time series is removed from the data.

[20] Again, it should be noted that while the 11 km box size is a reasonable upper bound on the location error in southern California, other box sizes may be used instead. Preliminary work suggests that larger box sizes, using the boolean formulation described above, reduces the effect of the more numerous smaller events, in particular those associated with aftershock sequences, but more work is necessary to confirm these results.

[21] In addition, varying the time step size will also affect the resulting eigenvectors. For example, tests show that using smaller time steps causes very little change in the lower eigenmodes in this particular case, suggesting that timescales on the order of a day define the lower limit of the temporal interactions in the southern California fault system. However, one can imagine that using larger time steps might lead to the discovery of modes with longer temporal correlations than those revealed in this analysis, such as those associated with viscoelastic relaxation, the time constant of which, in southern California, is on the order of several months to several years [Deng *et al.*, 1998; Pollitz *et al.*, 2001].

[22] For the time period 1932 through August 1999, the seismicity was analyzed using the entire data set, including the entire areal extent and events of all quality. The time interval for this decomposition was increased to one day, so that the total number of time steps is approximately 24,333. In addition, all locations from the entire database, and all quality events, were included, even those where no event occurred for the more than 67 years. The number of location time series affected by the seismicity, p , therefore is 3621.

[23] Figure 3 is a plot of the major earthquakes in California from 1932 through 1999 that will be discussed in the following sections. Included is the zone of seismicity associated with the Mammoth Mountain/Long Valley volcanic area in the northeast part of the state. Table 1 lists the sequence and date of those events shown in Figure 3.

Table 1. Major Earthquakes in California, 1932–1999^a

Event	Date	Mechanism
Long Beach	1933	strike-slip
Kern County	1952	strike-slip
Parkfield	1966	strike-slip
Borrego Mountain ^b	1968	strike-slip
San Fernando	1971	thrust
Imperial Valley	1979	strike-slip
Coalinga	1983	thrust
Superstition Hills/Elsinore Ranch	1987	strike-slip
Loma Prieta	1989	strike-slip
Landers ^c	1992	strike-slip
Northridge	1994	thrust
Hector Mine	1999	strike-slip

^aSee also Figure 3.

^bAdjacent to the San Jacinto event, 1954.

^cAssociated with the 1991 Joshua Tree and 1992 Big Bear earthquakes.

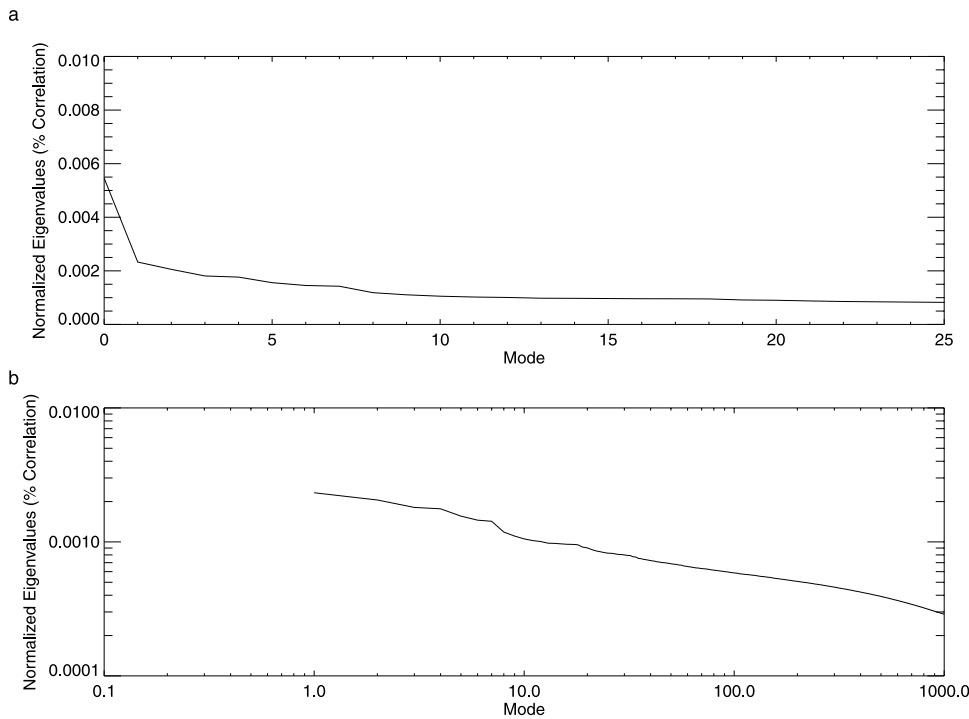


Figure 4. (a) First 25 eigenvalues, normalized to the sum of all eigenvalues, KLE analysis, 1932–1999.
(b) First 1000 normalized eigenvalues, plotted on a lognormal scale.

[24] For the time period 1932 to 1991, the time interval for the analysis was again one day, so that the total number of time steps is approximately 21,535. Again, all locations were included, even those where no event occurred for the entire 59 years. Results applied to the catalog with a magnitude cut of three, as well as no magnitude cut, will be shown. The total number of location time series remains constant at 3621.

4. Results and Discussion

4.1. Time Period: 1932 Through August 1999

[25] In our first analysis example, the time period starting in 1932 and continuing through the end August 1999 was analyzed using the entire data set, including the entire areal extent and events of all quality. Figure 4a is a plot of the first 25 normalized eigenvalues, while Figure 4b is the first 1000 normalized eigenvalues, plotted on a lognormal scale.

[26] Figure 5 shows the first two modes for southern California for this data set. These plots reflect the correlations in then seismicity, not the actual seismicity itself. The absolute maximum value in each plot is normalized to one, where red is positive and blue is negative; red and blue are anticorrelated. The correct interpretation is that while a red location is “on”, a blue location is “off”, and vice versa. The first mode is effectively a background hazard map, where small events are correlated with each other throughout southern California, while the second mode is the Landers event. The accompanying PC time series are shown in Figures 5a and 5c. The influence of spatial and temporal variations due to the density and completeness of network coverage is visible in the PC time series. For example, note

the distinctive wave associated with the Landers sequence and its large numbers of aftershocks, punctuated by the occurrence of the Northridge event. Again, this what we call the background, or detectability mode. In theory, there is no need to apply an arbitrary cutoff to the data set, with its accompanying uncertainty. It should be possible to simply quantify and remove this mode in order to study smaller, more influential modes. While this may not, as yet, be the optimal time series construction for this purpose, at the very least, in the future, one should be able to identify the influence of the network variability in time, space, and magnitude on the remaining modes.

[27] Figure 5d shows the second KLE mode. Here the region surrounding the 1992 Landers event is “on” (red) whereas the rest of the southern San Andreas fault system is “off” (blue). The Coalinga earthquake is visible in this mode, and an apparent correlation between Landers and a set of events in eastern Nevada is revealed.

[28] As can be seen in Figure 6, a number of the KLE eigenpatterns are lower-order harmonics of the second mode. Interestingly, Figure 6d, KLE7, illustrates the correlations between the North Palm Springs event of 1986, a 5.6 magnitude event located southeast of the Big Bear earthquake of 1992, and other major southern California earthquakes, but with minimal correlation with the nearby Landers sequence. Notice the Oceanside event, a magnitude 5.4 event that occurred off the southern coast of California in 1986, in KLE6 and KLE7, and a feature prominent in most of the lower KLE modes in this decomposition.

[29] Typically, the higher-order KLE modes display signal on shorter spatial and temporal scales than the initial, lower modes. This feature is illustrated in Figure 6. Figure 6e,

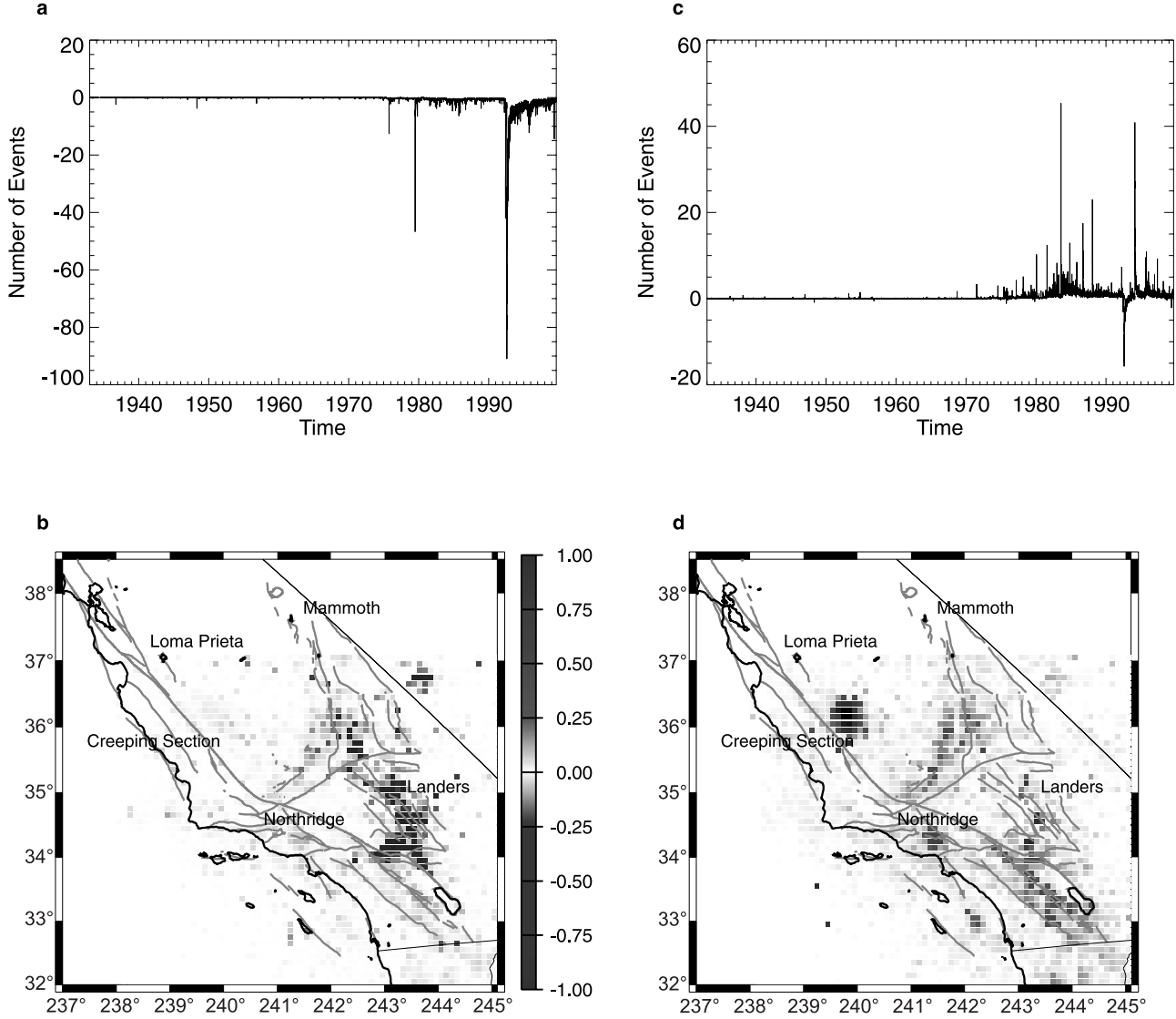


Figure 5. First two KLE modes for southern California seismicity, 1932–1999. (a) PC time series for first KLE mode, (b) first KLE mode, normalized to maximum, (c) PC time series for second KLE mode, and (d) second KLE mode, also normalized to the maximum. See color version of this figure at back of this issue.

KLE8, is a smaller-scale harmonic of Figure 6c, KLE6, while Figure 6f, KLE9, shows the Landers sequence, essentially isolated, with the Joshua Tree earthquake anticorrelated with the Landers event to the north and Big Bear to the northwest.

[30] Initial attempts to verify this method include creating random catalogs of two kinds. In the first, the catalog is randomized on both space and time, with the only requirement being that the locations of the randomized events remain on the existing fault structure, rather than over the entire grid. In the second case, the catalog is randomized in space in the same fashion but is not randomized in time, keeping, therefore, the temporal clustering associated with aftershock sequences. In the first case, the resulting eigenvectors are completely random, with little spatial signal above background noise, and none that is correlated with known temporal sequences. In the second, one or two

modes exist in which single sites are correlated with one or two other remote, single sites, as a result of random temporal correlations that remain after the spatial randomization. However, no apparent spatial relation remains based on either recognized tectonic activity or earthquake physics; for example, the spatial signal usually associated with aftershock sequences is undetectable. From this work we conclude that correlations do exist in the actual data, both spatial and temporal, that we are measuring in the decomposition shown above.

4.2. Time Period: 1932 Through December 1991

[31] One of the interesting questions which arises in studying the results above is how exactly the dominance of the Landers sequence, and its associated instrumentation, affects the eigenpatterns. This encouraged the removal of that event from the data set by cutting off the time series

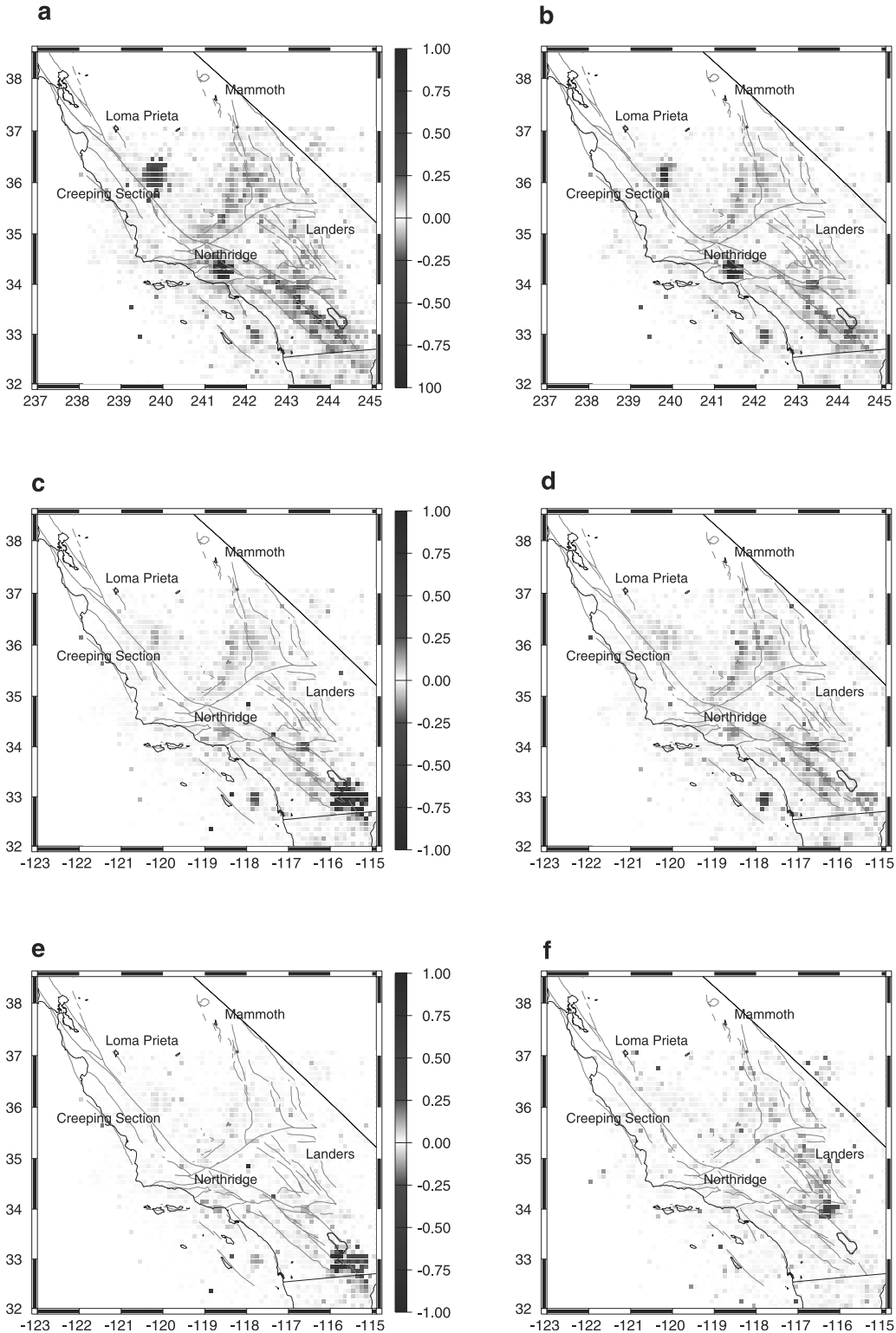


Figure 6. KLE modes three and four, six through nine, for southern California seismicity, 1932–1999, each normalized to the maximum. (a) Third KLE mode, normalized to maximum, (b) fourth KLE mode, (c) sixth KLE mode, (d) seventh KLE mode, (e) eighth KLE mode, and (f) ninth KLE mode. See color version of this figure at back of this issue.

before its occurrence, at the end of 1991. For this time period, 1932 to 1991, the time series interval was again one day, so that the total number of time steps is approximately 21,535. Again, all locations from the entire database, and all

quality events, were included in the decomposition, so that the number of location time series is 3621.

[32] Figure 7a shows the first 25 normalized eigenvalues, while Figure 7b is the first 1000 normalized eigenvalues,

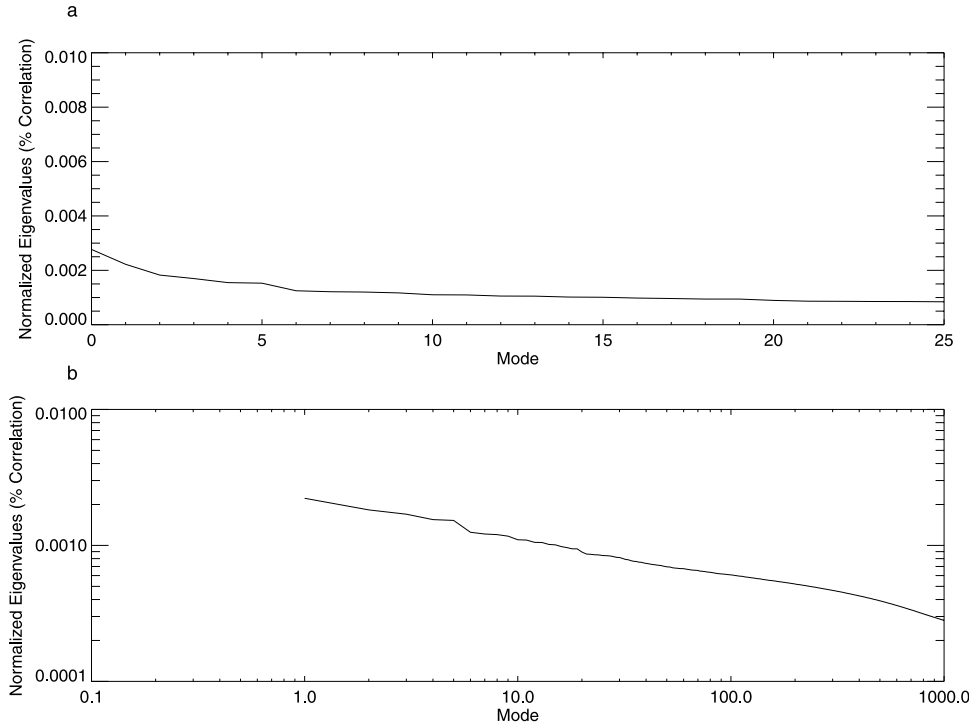


Figure 7. (a) First 25 eigenvalues, normalized to the sum of all eigenvalues, KLE analysis, 1932–1999.
(b) First 1000 normalized eigenvalues, plotted on a lognormal scale.

plotted on a lognormal scale. The eigenvalue plot is now smoother, without the large drop after the first mode which was a function of the large wave in the first PC time series generated by the Landers aftershocks (see Figure 5).

[33] KLE modes one and two are shown in Figure 8, where KLE1 is the mode associated with background seismicity. Note that many of what were the lower modes in the previous analysis have moved up in the eigenvalue ranking, replacing the large number of Landers harmonics. Figure 8b, KLE2, is now the 1983 Coalinga earthquake, anticorrelated with the 1986 Oceanside and North Palm Spring events. The 1971 San Fernando event is a single blue box, correlated with the Coalinga earthquake.

[34] The fourth KLE mode shown in Figure 8c is the 1987 Superstition Hills and Elsinore ranch events correlated with the Whittier Narrows earthquake and anticorrelated with the North Palm Springs and Oceanside events. Figure 8d, KLE mode five, also shows the North Palm Springs and Oceanside events correlated with each other, while in Figure 8e, KLE7, Point Mugu, a magnitude 5.3 earthquake that occurred in 1973 just off the coast south of Northridge appears correlated with the 1971 San Fernando event. The 1979 Homestead Valley earthquake sequence, a series of magnitudes 4 and 5 that occurred near the future Landers event, is also correlated with these events, while Imperial Valley is anticorrelated.

[35] Figure 8f, KLE8, again shows the 1979 Homestead Valley events, now anticorrelated with Point Mugu. Note the arcuate structure, which cuts across the faults at the location of the 1992 Landers earthquake. This is a feature of the local seismicity that has only been recognized in recent years with the occurrence of the 1991 Landers sequence and the 1999 Hector Mine earthquake, but which was clearly

visible in this decomposition as early as 1991 (Figure 8f). It should be noted again that no seismicity data after December 1991 are included in this analysis.

[36] Analysis of this same data set, 1932 through 1991, but with a magnitude cut of 3.0 applied to the data, yields KLE modes such as those shown in Figure 9. Note that the application of a magnitude cut has allowed events from earlier in the data set to have a greater prominence, and has reduced the number of harmonic modes in the upper eigenvectors. Interestingly, while the background mode has dropped out, as would be expected, the first mode is not Coalinga, the second mode in the entire data set (see Figure 8b), but the 1971 San Fernando event. This suggests that the exact magnitude cutoff chosen directly affects the eigenpattern decomposition sequence, probably by emphasizing or deemphasizing the aftershock sequences of the major events.

[37] The 1983 Coalinga earthquake is now the third KLE mode, behind the 1969 Avila Beach earthquake (see Figure 9). The correlation between the 1979 Imperial Valley and 1987 Superstition Hills sequence is the fourth mode. The 1952 Kern County earthquake has appeared in this decomposition as the seventh mode (Figure 9e). Figure 9f also shows KLE mode 11, one interesting feature of which is the anticorrelation between the 1983 Coalinga event and the historic location of the Parkfield earthquake to the west, which has not taken place in recent years as expected [Turcotte, 1997]. This mode supports speculation that the Coalinga event delayed the Parkfield event, which previously occurred at regular 22 year intervals.

4.3. Precursory Modes

[38] The presence of both large- and small-scale correlations in the data, evident in the KLE decompositions shown

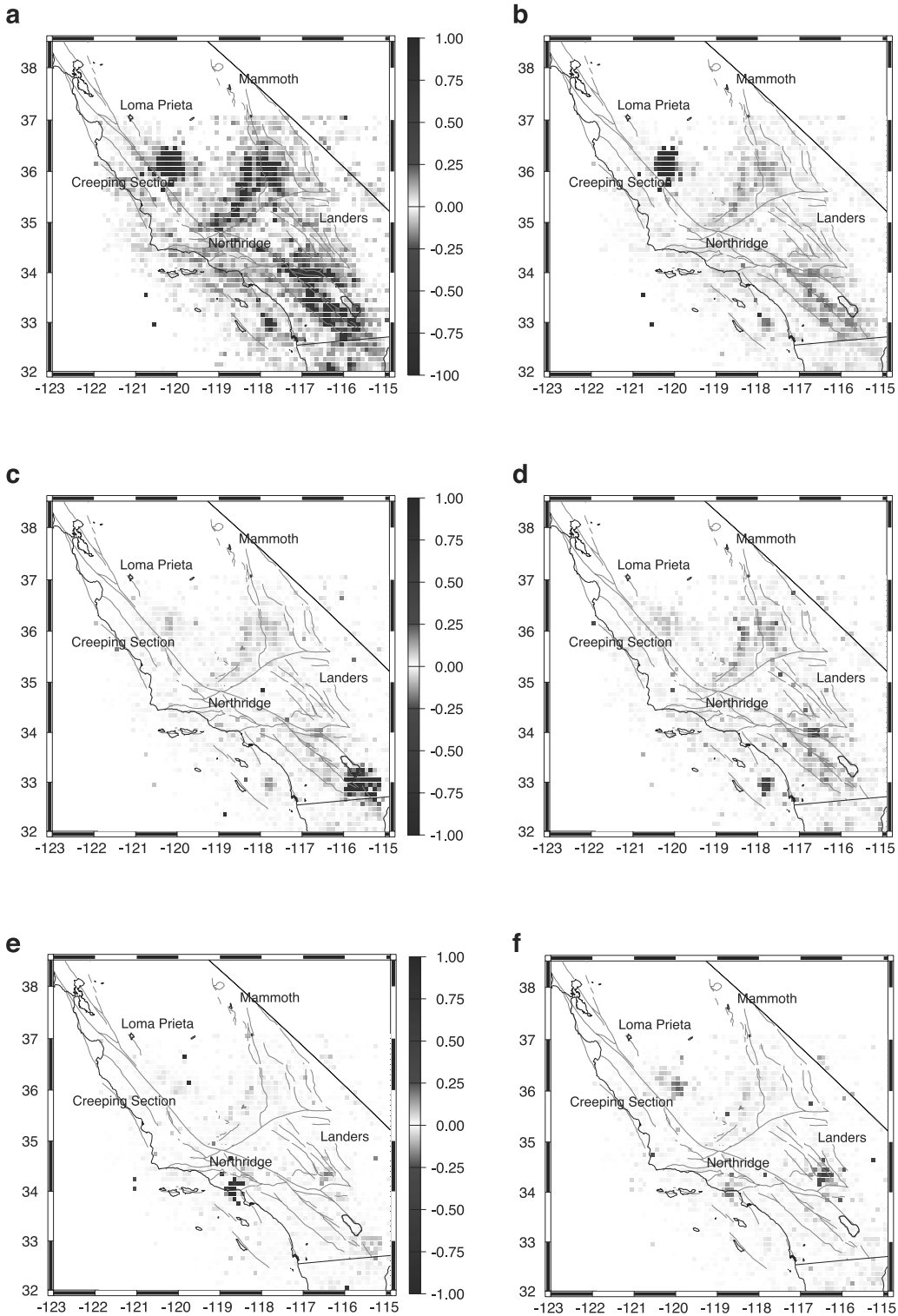


Figure 8. First two KLE modes, in addition to modes four, five, seven, and eight, for southern California seismicity, 1932–1991, normalized to the maximum. (a) First KLE mode, (b) second KLE mode, (c) fourth KLE mode, (d) fifth KLE mode, (e) seventh KLE mode, and (f) eighth KLE mode. See color version of this figure at back of this issue.

above, prompted a study of the change in these modes for each year, in an attempt to identify modes which consistently appear over some identifiable time period prior to an event. While a complex rate correlation operator, $K(\mathbf{x}_i, \mathbf{x}_j)$, can be

used to compute the probability of future events on a fault patch model producing events over time periods of thousands of years [Rundle et al., 2000], its application to historic seismicity data is limited. Neither the long time periods nor

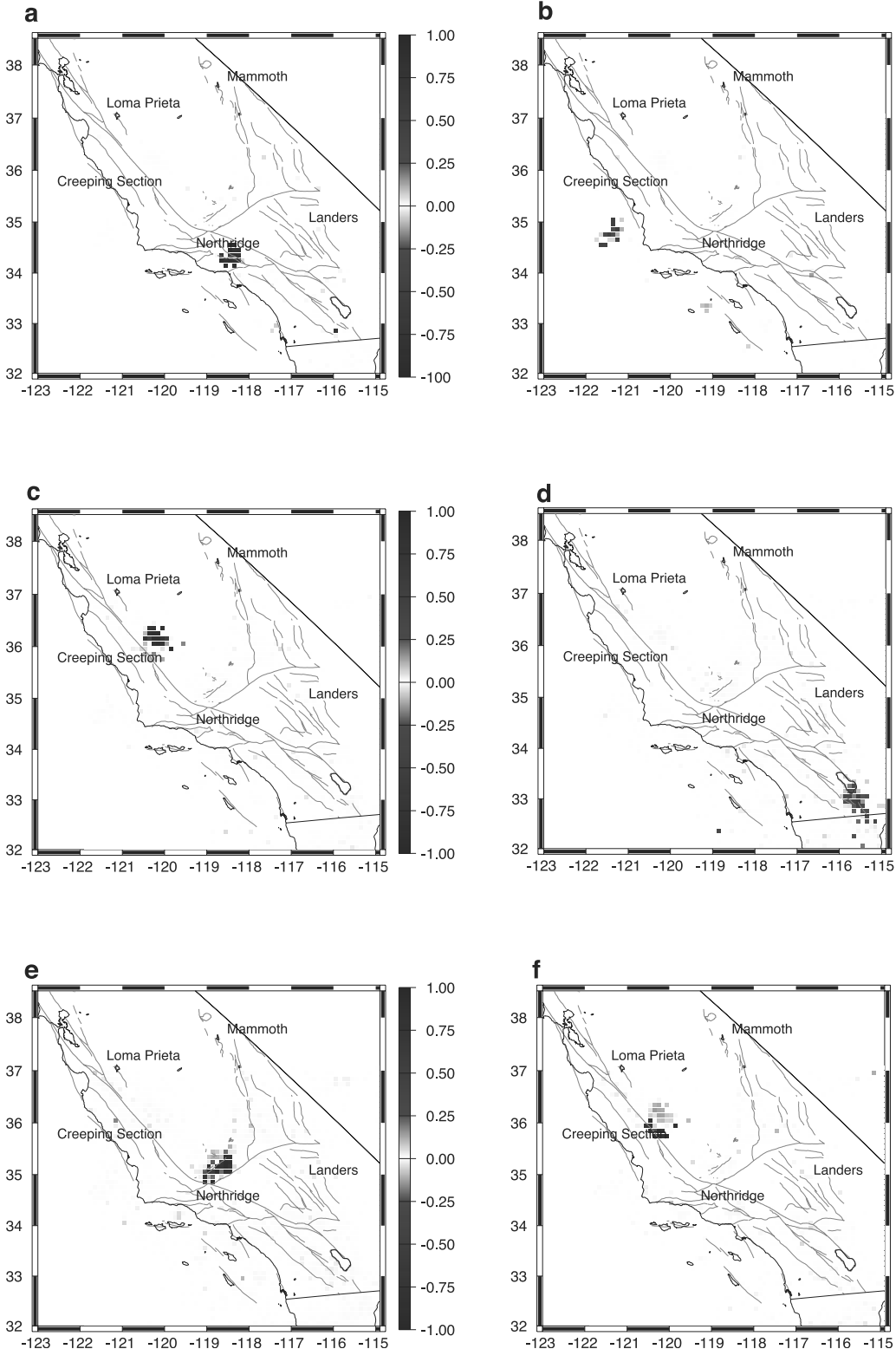


Figure 9. (a) First KLE mode, (b) second KLE mode, (c) third KLE mode, (d) fourth KLE mode, (e) seventh KLE mode, and (f) eleventh KLE mode for southern California seismicity, $M < 3.0$, 1932–1991, each normalized to its maximum. See color version of this figure at back of this issue.

the large number of moderate to large events produced by numerical simulations are available in the actual data, nor is the same accuracy in time and space possible. Consequently, the following method was developed.

[39] If the seismicity in a given year, S , is known, and the eigenmodes, or eigenvectors e_i , are calculated using all seismicity data (a total of $i = 1, \dots, N$ sites), then the eigenvectors are a complete, orthonormal set of basis

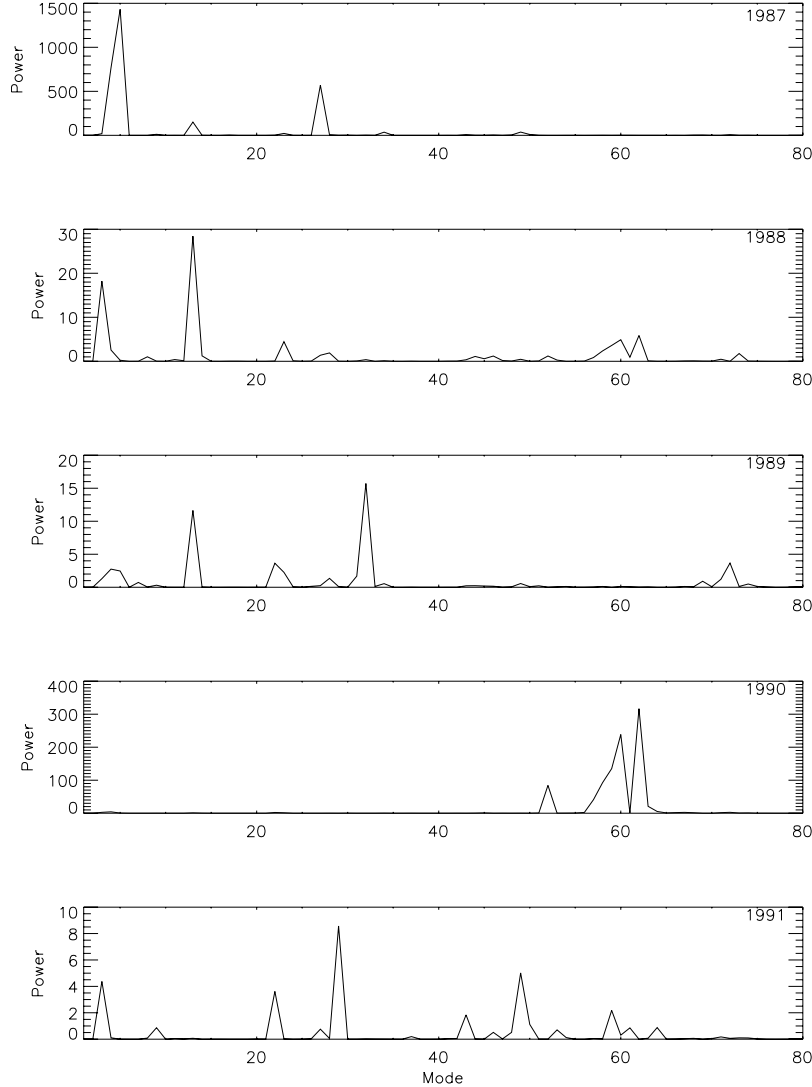


Figure 10. Eigenvalue power for the individual years 1987–1991, decomposed using eigenmodes derived from southern California seismicity, $M > 3.0$, 1932–1991.

functions, and any seismicity over that space can be decomposed into those eigenvectors.

$$S = \sum_{i=1}^N \alpha_i e_{ji},$$

where α_i are the eigenvalues for that particular year. The eigenvalues, α_i , are then computed from

$$\alpha_i = \sum_{i=1}^N e_{ji} S_i.$$

Computing the α_i for any given year, given the KLE decompositions above, is a relatively simple process. The data set used was that described above, for the time period 1932 through 1991, with a magnitude cutoff of 3.0. The resulting α_i^2 , i.e., the power spectrum for the eigenmodes, for each year prior to the 1992 Landers sequence, are plotted in Figure 10. Note again, that no data after December 1991 are included in this analysis. Events that occur in the data set, for example, the 1979 Imperial Valley event or the 1983 Coalinga

earthquake, have signal in the corresponding eigenmodes, and would be expected to produce signal prior to those events. In addition, several of the higher-order eigenmodes, on smaller spatial and temporal scales, appear to change in a large way over the several years prior to 1992. Interestingly, a number of the modes that increase are those that include signal for the 1992 Landers earthquake sequence. For example, Figures 11a–11c show KLE modes 49, 58, and 62, which, while noisy, contain significant correlations for the Joshua Tree, Landers, and Big Bear events.

[40] Figure 12 shows the α_i^2 , plotted for the seismicity over each year, summed sequentially from 1987 through 1991. Systematic changes now appear in the α_i^2 . These show the growth in the smaller-scale Landers modes over time, as the fault system becomes increasingly correlated prior to the 1992 event. Zoller et al. [2001] also observe growing correlation lengths over time for large events in southern California. Again, it is important to remember that no data after 31 December 1991 are included in the analysis of either these eigenmodes or the associated α_i^2 .

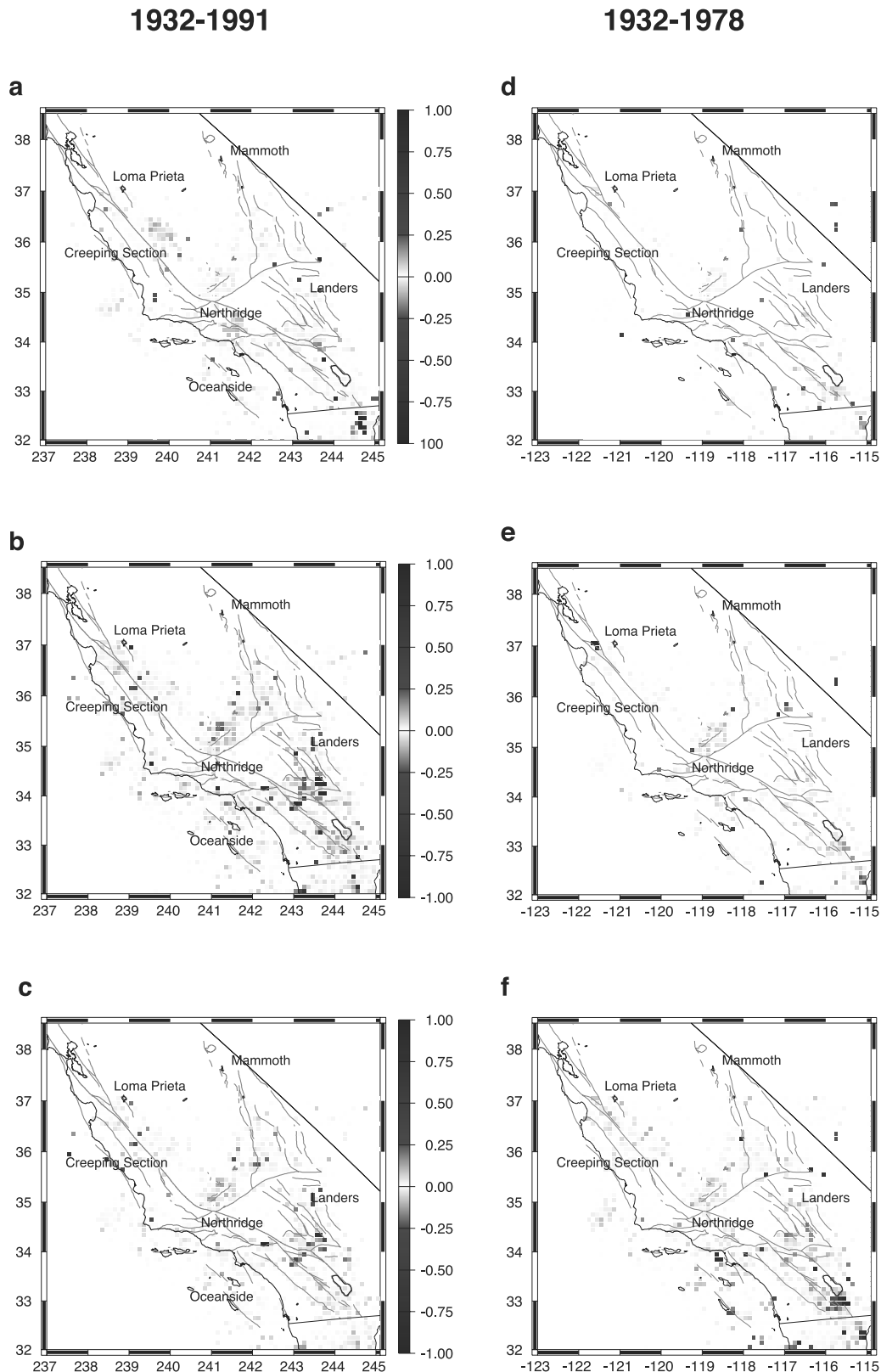


Figure 11. (a) KLE mode 49, (c) KLE mode 58, and (d) KLE mode 62 for southern California seismicity, $M > 3.0$, 1932–1991, each normalized to its maximum. For 1932–1978, (d) KLE mode, (e) KLE mode, and (f) KLE mode 62, southern California seismicity, $M > 3.0$, each normalized to its maximum. See color version of this figure at back of this issue.

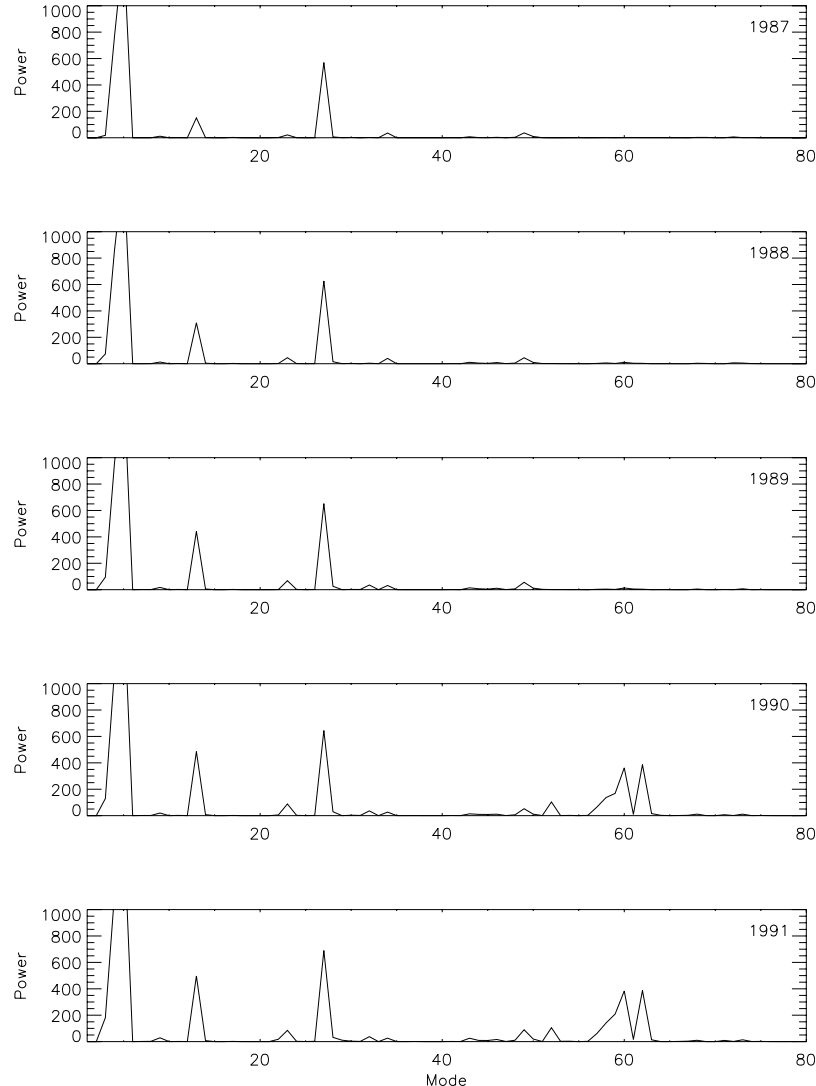


Figure 12. Eigenvalue power summed from 1987 through 1991, decomposed using eigenmodes derived from southern California seismicity, $M > 3.0$, 1932–1991.

[41] Figure 13 shows the α_i^2 , plotted for the seismicity over each year, this time plotted for the summation from 1974 through 1978. The Imperial Valley earthquake, $M = 6.4$, occurred on 15 October 1979. Systematic changes can be seen in this plot as well, reinforcing the connection between the correlated, small-scale, short-time eigenmodes shown in Figures 11d–11f and the upcoming event. In this decomposition, no data after 31 December 1978 are included in the analysis.

[42] Note that this eigenvalue decomposition corresponds to a multidimensional vector, formed from the seismic activity by assuming that each of the locations on the grid of southern California is one of the dimensions. If the seismicity patterns, as described by the correlations in the α_i^2 , are undergoing a systematic change due to the growth of precursory modes, such as seen in Figures 11, 12, and 13, then the vector is no longer experiencing a random walk about some mean, but undergoes a persistent walk away from that mean. Future work will study the implications of this persistent change, and will include a systematic test of this

method against all large events in southern California in order to confirm its success rate. The important point here in studying these summed modes is to remember that, in constructing the original decomposition modes, only catalog data up until 31 December 1978 and 31 December 1991, respectively, were included in the analysis. In other words, no information from the upcoming Imperial Valley earthquake of 1979 or the Landers sequence of 1991 was used to construct the precursory modes.

5. Conclusions

[43] This pattern dynamics approach that we have applied to historical seismicity data in southern California reveals a wealth of interesting spatial patterns. In particular, it provides a new methodology for classifying all of the possible seismicity patterns that can exist in the actual catalog in terms of the mutually orthogonal eigenstates of a set of boolean activity functions in space and time. In fact, a number of the descriptive patterns cited earlier can be

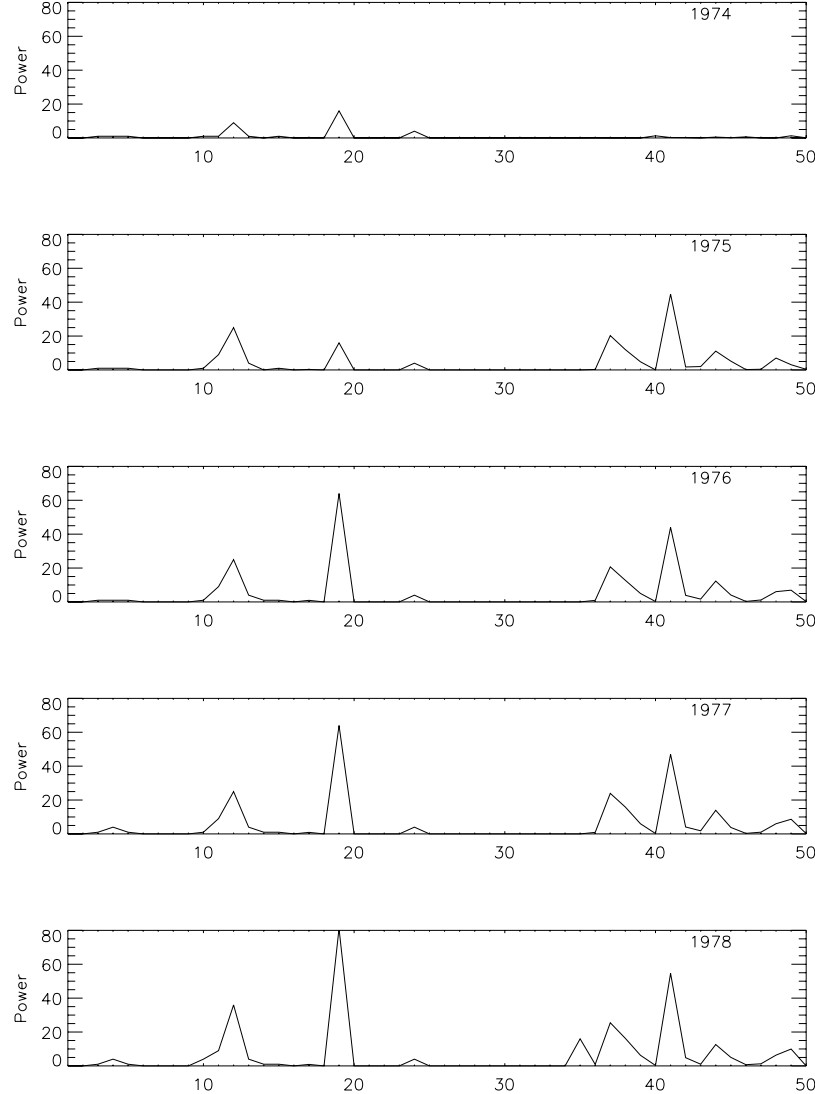


Figure 13. Eigenvalue power summed from 1974 through 1978, decomposed using eigenmodes derived from southern California seismicity, $M > 3.0$, 1932–1978.

readily identified among the eigenstates depicted in Figures 5 through 11. For example, Figure 5d can be interpreted either as seismic activation within the Landers epicentral region, or else as quiescence near Landers coincident with seismic activity surrounding the region, i.e., a “Mogi donut.” Although the historic data set is clearly not long enough to accurately identify all the primary modes that characterize seismicity over the last several thousand years within the region, our analysis nonetheless illustrates the utility of these methods.

[44] Several issues still remain to be studied. For example, there appear to be no correlations in the lower eigenmodes for certain events, such as the 1918 San Jacinto event that occurred northwest of Borrego Mountain. Yet there are small-scale correlations with that location, albeit noisy, in modes corresponding to eigenvalues in the mid-50s, in the analysis on data sets with no cutoff, even though this event does not occur in the historic data set. Questions arise as to the importance of these small-scale correlations and their significance level in the precursory modes. Associated with

this issue is the necessity of determining either the correct magnitude cutoff value, or the appropriate method for removing uninteresting modes associated with the network variability. Not that, until this issue is resolved, it is difficult to comment on the potential lack of correlation between events, as there are over 3621 possible eigenpatterns to study for each decomposition. The possibility that those correlations might be on a smaller spatial or temporal scale than the lower eigenmodes is not surprising if one understands the physics of the earthquake system, as discussed in the next paragraph. The scales, i.e., the eigenvalue of the mode of interest, may contain important information about the processes that determine the correlations.

[45] This technique shows additional promise for the study of both length and timescales that are directly related to the physics of earthquake fault systems. As discussed above, there are a variety of length scales of interest in the southern California region. For example, while the seismogenic zone is between 15 and 25 km [Pollitz *et al.*, 2001], the aftershock region is generally substantially larger [Gross

and Kisslinger, 1994], correlation lengths of several hundred kilometers are expected for large events [Bowman *et al.*, 1998; Zoller *et al.* 2001], and dynamic triggering of earthquakes over distances spanning almost 500 km has been detected [Hill *et al.*, 1995]. In addition, timescales ranging from hours to years for aftershock sequences [Gross and Kisslinger, 1994], months for viscoelastic response [Pollitz *et al.*, 2001], and years for foreshock sequences [Bowman *et al.*, 1998] are typical, just to name a few physical mechanisms in the fault system. This method will be used in the future to study the regions and scales of interest for these and other underlying mechanisms.

[46] Our results argue strongly for the development of realistic numerical simulations of fault systems such as those in southern California [Rundle, 1988; Tiampo *et al.*, 1999; Rundle *et al.*, 2000]. Because the historic data set is incomplete worldwide, construction of such numerical simulations is necessary to more accurately define the most significant eigenpatterns, which can be applied to understanding the nature of the observed seismicity. Moreover, such simulations will be of critical importance for relating the observable pattern basis set for the seismicity data to the pattern basis set for stress, strains, and displacements through time. While seismicity is readily observable by standard methods, stress and strain within the earth are not. However, stress and strain are the primary dynamical variables, and are also the Markov variables in which the underlying nonlinear dynamics are almost certainly formulated. It will be most important to relate a readily observable, seismicity pattern basis set to the actual, unobservable dynamical pattern basis set, so that mode-shaping techniques can be applied to the underlying dynamics [Fukunaga, 1970; Holmes *et al.*, 1996]. In this manner it may be possible to characterize the spatially coarse-grained features of local and regional stress levels, coefficients of friction, failure and residual stress levels, and fault interactions. Finally, Rundle *et al.* [2000], demonstrated using simulations that such methods can in principle forecast future events with accuracies considerably better than a standard Poisson process.

[47] With the development of a quantitative, readily reproducible technique for characterizing all possible seismicity patterns, these methods may allow us to test the hypothesis that large damaging earthquakes on a given subset of faults are preceded by one of a small set of characteristic precursory seismicity patterns. If this hypothesis is true, then it may well be possible to develop a quantitative method to forecast large, infrequent events using the patterns of seismic activation and quiescence associated with smaller, more frequent events on local and regional fault systems.

[48] **Acknowledgments.** This research was supported by CIRES and NASA student fellowships (K.F.T. and S.M.), by U.S. DOE grant DE-FG03-95ER14499 (J.B.R.), by NASA grant NAG5-5168 (S.J.G.), and by U.S. DOE grant DE-FG02-95ER14498 (W.K.). This work was also supported by the Southern California Earthquake Center (K.F.T.). SCEC is funded by NSF Cooperative Agreement EAR-8920136 and USGS Cooperative Agreements 14-08-0001-A0899 and 1434-HQ-97AG01718. This is SCEC contribution 702.

References

- Aubrey, D. G., and K. O. Emery, Eigenanalysis of recent United States sea levels, *Cont. Shelf Res.*, 2, 21–33, 1983.
- Bak, P., C. Tang, and K. Weisenfeld, Self-organized criticality: An explanation of the $1/f$ noise, *Phys. Rev. Lett.*, 59, 381–384, 1987.
- Bakun, W. H., and T. V. McEvilly, Recurrence models and Parkfield, California, earthquakes, *J. Geophys. Res.*, 89, 3051–3058, 1984.
- Bakun, W. H., G. C. P. King, and R. S. Cockerham, Seismic slip, aseismic slip, and the mechanics of repeating earthquakes on the Calaveras fault, California, in *Earthquake Source Mechanics*, *Geophys. Monogr. Ser.*, vol. 37, edited by S. Das, J. Boatwright, and C. H. Schlotz, pp. 195–208, AGU, Washington, D.C., 1986.
- Bowman, D. D., G. Ouillon, C. G. Sammis, A. Sornette, and D. Sornette, An observational test of the critical earthquake concept, *J. Geophys. Res.*, 103, 24,359–24,372, 1998.
- Brehm, D. J., and L. W. Braile, Intermediate-term earthquake prediction using the modified time-to-failure method in southern California, *Bull. Seismol. Soc. Am.*, 89, 275–293, 1999.
- Bufe, C. G., and D. J. Varnes, Predictive modeling of the seismic cycle of the greater San Francisco bay region, *J. Geophys. Res.*, 98, 9871–9883, 1993.
- Deng, J. S., and L. R. Sykes, Triggering of 1812 Santa Barbara earthquake by a great San Andreas shock: Implications for future hazards in southern California, *Geophys. Res. Lett.*, 23, 1155–1158, 1996.
- Deng, J., M. Gurnis, H. Kanamori, and E. Hauksson, Viscoelastic flow in the lower crust after the 1992 Landers, California, earthquake, *Science*, 282, 1689–1692, 1998.
- Dieterich, J. H., A constitutive law for rate of earthquake production and an application to earthquake clustering, *J. Geophys. Res.*, 99, 2601–2618, 1994.
- Dodge, D. A., G. C. Beroza, and W. L. Ellsworth, Detailed observations of California foreshock sequences: Implications for the earthquake initiation process, *J. Geophys. Res.*, 101, 22,371–22,392, 1996.
- Ellsworth, W. I., and A. T. Cole, A test of the characteristic earthquake hypothesis for the San Andreas Fault in central California, *Seismol. Res. Lett.*, 68, 298, 1997.
- Eneva, M., and Y. Ben-Zion, Techniques and parameters to analyze seismicity patterns associated with large earthquakes, *J. Geophys. Res.*, 102, 17,785–17,795, 1997.
- Ferguson, C., W. Klein, and J. B. Rundle, Spinodals, scaling and ergodicity in a model of an earthquake fault with long-range stress transfer, *Phys. Rev. E*, 60, 1359–1373, 1999.
- Fisher, D. S., K. Dahmen, S. Ramanathan, and Y. Ben-Zion, Statistics of earthquakes in simple models of heterogeneous faults, *Phys. Rev. Lett.*, 78, 4885–4888, 1997.
- Frohlich, C., Aftershocks and temporal clustering of deep earthquakes, *J. Geophys. Res.*, 92, 13,944–13,956, 1987.
- Fukunaga, K., *Introduction to Statistical Pattern Recognition*, Academic, San Diego, Calif., 1970.
- Garcia, A., and C. Penland, Fluctuating hydrodynamics and principal oscillation pattern analysis, *J. Stat. Phys.*, 64, 1121–1132, 1991.
- Gomberg, J., Stress/strain changes and triggered seismicity following the M_w 7.3 Landers, California, earthquake, *J. Geophys. Res.*, 101, 751–764, 1996.
- Grant, L., and K. Sieh, Paleoseismic evidence of clustered earthquakes on the San Andreas fault in the Carrizo Plain, *J. Geophys. Res.*, 99, 6819–6842, 1994.
- Gross, S. J., and C. Kisslinger, Tests of models of aftershock rate decay, *Bull. Seismol. Soc. Am.*, 84, 1571–1579, 1994.
- Gross, S., and J. B. Rundle, A systematic test of time-to-failure analysis, *Geophys. J. Int.*, 133, 57–64, 1998.
- Haberman, R. E., Precursory seismicity patterns: Stalking the mature seismic gap, in *Earthquake Prediction: An International Review*, Maurice Ewing Ser., vol. 4, edited by D. W. Simpson and P. G. Richards, pp. 29–42, AGU, Washington, D. C., 1981.
- Hertz, J., A. Korgh, and R. G. Palmer, *Introduction to the Theory of Neural Computation, Lect. Notes*, vol. I, Addison-Wesley-Longman, Reading, Mass., 1990.
- Herz, A. V., and J. J. Hopfield, Earthquake cycles and neural reverberations: Collective oscillations in systems with pulse-coupled threshold elements, *Phys. Rev. Lett.*, 75, 1222–1225, 1995.
- Hill, D., J. P. Eaton, and L. M. Jones, Seismicity, 1980–86, in *The San Andreas Fault System, California, U.S. Geol. Surv. Prof. Pap.*, 1515, 115–152, 1990.
- Hill, D. P., et al., Seismicity remotely triggered by the magnitude 7.3 Landers, California, earthquake, *Science*, 260, 1617–1623, 1993.
- Hill, D. P., M. J. S. Johnston, J. O. Langbein, and R. Bilham, Response of Long Valley caldera to the M_w = 7.3 Landers, California, earthquake, *J. Geophys. Res.*, 100, 12,985–13,005, 1995.
- Holmes, P., J. L. Lumley, and G. Berkooz, *Turbulence, Coherent Structures, Dynamical Systems and Symmetry*, Cambridge Univ. Press, New York, 1996.
- Hotelling, H., Analysis of a complex of statistical variables into principal components, *J. Educ. Psych.*, 24, 417–520, 1933.

- House, L. S., L. R. Sykes, J. N. Davies, and K. H. Jacob, Identification of a possible seismic gap near Unalaska Island, eastern Aleutians, Alaska, in *Earthquake Prediction: An International Review, Maurice Ewing Ser.*, vol. 4, edited by D. W. Simpson and P. G. Richards, pp. 81–92, AGU, Washington, D. C., 1981.
- Huang, Y., H. Saleur, C. Sammis, and D. Sornette, Precursors, aftershocks, criticality and self-organized criticality, *Europhys. Lett.*, 41, 43–49, 1998.
- Jaume, S. C., and L. R. Sykes, Evolving towards a critical point: A review of accelerating seismic moment/energy release prior to large and great earthquakes, *Pure Appl. Geophys.*, 155, 279–306, 1999.
- Jones, L. M., and E. Hauksson, The seismic cycle in southern California: Precursor or response?, *Geophys. Res. Lett.*, 24, 469–472, 1997.
- Kagan, Y. Y., and D. D. Jackson, Seismic gap hypothesis, 10 years after, *J. Geophys. Res.*, 96, 21,419–21,431, 1992.
- Kanamori, H., The nature of seismicity patterns before large earthquakes, in *Earthquake Prediction: An International Review, Maurice Ewing Ser.*, vol. 4, edited by D. W. Simpson and P. G. Richards, pp. 1–19, AGU, Washington, D. C., 1981.
- Kato, N., M. Ohtake, and T. Hirasawa, Possible mechanism of precursory seismic quiescence: Regional stress relaxation due to preseismic sliding, *Pure Appl. Geophys.*, 150, 249–267, 1997.
- Kerr, R. A., A slow start for earthquakes, *Science*, 279, 985, 1998.
- King, G. C. P., R. S. Stein, and J. Lin, Static stress changes and the triggering of earthquakes, *Bull. Seismol. Soc. Am.*, 84, 935–953, 1994.
- Linde, A. T., M. T. Gladwin, M. J. S. Johnston, R. L. Gwyther, and R. G. Bilham, A slow earthquake sequence on the San Andreas fault, *Nature*, 383, 65–68, 1996.
- Lyzenga, G. A., A. Raefsky, and S. G. Mulligan, Models of recurrent strike-slip earthquake cycles and the state of crustal stress, *J. Geophys. Res.*, 96, 21,623–21,640, 1991.
- Marone, C., J. E. Vidale, and W. L. Ellsworth, Fault healing inferred from time-dependent variations in source properties of repeating earthquakes, *Geophys. Res. Lett.*, 22, 3095–3098, 1995.
- McGuire, J. J., P. F. Imhle, and T. H. Jordan, Time-domain observations of a slow precursor to the 1994 Romanche transform earthquake, *Science*, 274, 82–85, 1996.
- Moghaddam, B., W. Wahid, and A. Pentland, Beyond eigenfaces: Probabilistic matching for face recognition, paper presented at Third IEEE International Conference on Automatic Face and Gesture Recognition, Nara, Japan, 14–16 April 1998.
- Mogi, K., Some features of recent seismic activity in and near Japan, (2) Activity before and after great earthquakes, *Bull. Earthquake Res. Inst. Univ. Tokyo*, 47, 395–417, 1969.
- Nanjo, K., H. Nagahama, and M. Satomura, Rates of aftershock decay and the fractal structure of active fault systems, *Tectonophysics*, 287, 173–186, 1998.
- Nijhout, H. F., Pattern formation in biological systems, *Pattern Formation in the Physical and Biological Sciences, Lect. Notes*, vol. V, pp. 269–298, Addison-Wesley-Longman, Reading, Mass., 1997.
- North, G. R., Empirical orthogonal functions and normal modes, *J. Atmos. Sci.*, 41(5), 879–887, 1984.
- Ouchi, T., Population dynamics of earthquakes and mathematical modeling, *Pure Appl. Geophys.*, 140, 15–28, 1993.
- Pacheco, J. F., C. H. Scholz, and L. R. Sykes, Changes in frequency-size relationship from small to large earthquakes, *Nature*, 355, 71–73, 1992.
- Penland, C., Random forcing and forecasting using principal oscillation pattern analysis, *Mon. Weather Rev.*, 117, 2165–2185, 1989.
- Penland, C., and T. Magorian, Prediction of Niño 3 sea surface temperatures using linear inverse modeling, *J. Clim.*, 6, 1067–1076, 1993.
- Penland, C., and P. D. Sardeshmukh, The optimal growth of tropical sea surface temperature anomalies, *J. Clim.*, 8, 1999–2024, 1995.
- Pollitz, F. F., and I. S. Sacks, The 1995 Kobe, Japan, earthquake: A long-delayed aftershock of the offshore 1944 Tonankai and 1946 Nankaido earthquakes, *Bull. Seismol. Soc. Am.*, 87, 1–10, 1997.
- Pollitz, F. F., C. Wicks, and W. Thatcher, Mantle flow beneath a continental strike-slip fault: Postseismic deformation after the 1999 Hector Mine earthquake, *Science*, 293, 1814–1817, 2001.
- Preisendorfer, R. W., *Principle Component Analysis in Meteorology and Oceanography*, Elsevier Sci., New York, 1988.
- Press, F., and C. Allen, Patterns of seismic release in the southern California region, *J. Geophys. Res.*, 100, 6421–6430, 1995.
- Press, W. H., B. P. Flannery, S. A. Teukolsky, and W. T. Vettering, *Numerical Recipes in C*, 2nd ed., Cambridge Univ. Press, New York, 1992.
- Romanowicz, B., and J. B. Rundle, On scaling relations for large earthquakes, *Bull. Seismol. Soc. Am.*, 83, 1294–1297, 1993.
- Rundle, J. B., A physical model for earthquakes: 2. Applications to southern California, *J. Geophys. Res.*, 93, 6255–6274, 1988.
- Rundle, J. B., Derivation of the complete Gutenberg-Richter magnitude-frequency relation using the principle of scale invariance, *J. Geophys. Res.*, 94, 12,337–12,342, 1989.
- Rundle, J. B., Magnitude-frequency relation for earthquakes using a statistical mechanical approach, *J. Geophys. Res.*, 98, 21,943–21,950, 1993.
- Rundle, J. B., and W. Klein, New ideas about the physics of earthquakes, *U.S. Natl. Rep. Int. Union Geod. Geophys.*, 1991–1994, *Rev. Geophys.*, 33, 283–286, 1995.
- Rundle, J. B., S. Gross, W. Klein, C. Ferguson, and D. L. Turcotte, The statistical mechanics of earthquakes, *Tectonophysics*, 277, 147–164, 1997.
- Rundle, J. B., W. Klein, and S. Gross, Physical basis for statistical patterns in complex earthquake populations: Models, predictions and tests, *Pure Appl. Geophys.*, 155, 575–607, 1999.
- Rundle, J. B., W. Klein, K. Tiampo, and S. Gross, Linear pattern dynamics in nonlinear threshold systems, *Phys. Rev. E*, 61, 2418–2432, 2000.
- Saleur, H., C. G. Sammis, and D. Sornette, Discrete scale invariance, complex fractal dimensions, and log-periodic fluctuations in seismicity, *J. Geophys. Res.*, 17,661–17,677, 1995.
- Savage, J. C., Principal component analysis of geodetically measured deformation in Long Valley caldera, eastern California, 1983–1987, *J. Geophys. Res.*, 93, 13,297–13,305, 1988.
- Savage, J. C., The Parkfield prediction fallacy, *Bull. Seismol. Soc. Am.*, 83, 1–6, 1993.
- Scholz, C. H., *The Mechanics of Earthquakes and Faulting*, Cambridge Univ. Press, New York, 1990.
- Sieh, K., M. Stuiver, and D. Brillinger, A more precise chronology of earthquakes produced by the San Andreas fault in southern California, *J. Geophys. Res.*, 94, 603–623, 1989.
- Stark, M. A., and S. D. Davis, Remotely triggered microearthquakes at The Geysers geothermal field, California, *Geophys. Res. Lett.*, 23, 945–948, 1996.
- Stein, R. S., The role of stress transfer in earthquake occurrence, *Nature*, 402, 605–609, 1999.
- Stein, R. S., G. C. P. King, and J. Lin, Change in failure stress on the southern San Andreas fault system caused by the 1992 magnitude = 7.4 Landers earthquake, *Science*, 258, 1328–1331, 1992.
- Swan, F. H., D. P. Schwartz, and L. S. Cluff, Recurrence of moderate to large magnitude earthquakes produced by surface faulting on the Wasatch fault zone, Utah, *Bull. Seismol. Soc. Am.*, 70, 1431–1462, 1980.
- Tiampo, K. F., J. B. Rundle, W. Klein, and S. J. Gross, Systematic evolution of nonlocal space-time earthquake patterns in southern California, *Eos Trans. AGU*, 80(46), F1013, Fall Meet. Suppl., 1999.
- Tiampo, K. F., J. B. Rundle, S. McGinnis, S. J. Gross, and W. Klein, Observation of systematic variations in non-local seismicity patterns from southern California, in *GeoComplexity and the Physics of Earthquakes, Geophys. Monogr. Ser.*, vol. 120, edited by J. B. Rundle, D. L. Turcotte, and W. Klein, pp. 211–218, AGU, Washington, D. C., 2000.
- Turcotte, D. L., *Fractals and Chaos in Geology and Geophysics*, 2nd ed., Cambridge Univ. Press, New York, 1997.
- Vautard, R., and M. Ghil, Singular spectrum analysis in nonlinear dynamics, with applications to paleodynamic time series, *Physica D*, 35, 395–424, 1989.
- Wyss, M., and S. Wiemer, How can one test the seismic gap hypothesis? The case of repeated ruptures in the Aleutians, *Pure Appl. Geophys.*, 155, 259–278, 1999.
- Wyss, M., K. Shimazaki, and T. Urabe, Quantitative mapping of a precursory seismic quiescence to the Izu-Oshima 1990 ($M_{6.5}$) earthquake, Japan, *Geophys. J. Int.*, 127, 735–743, 1996.
- Wyss, M., D. Schorlemmer, and S. Wiemer, Mapping asperities by minima of local recurrence time: San Jacinto-Elsinore fault zones, *J. Geophys. Res.*, 105, 7829–7844, 2000.
- Yamashita, T., and L. Knopoff, A model of foreshock occurrence, *Geophys. J.*, 96, 389–399, 1989.
- Zoller, G., S. Hainzl, and J. Kurths, Observation of growing correlation length as an indicator for critical point behavior prior to large earthquakes, *J. Geophys. Res.*, 106, 2167–2175, 2001.

S. J. Gross, S. McGinnis, and K. F. Tiampo, CIRES, University of Colorado, Campus Box 216, Boulder, CO 80309-0216, USA. (sjg@quake.colorado.edu; sethmcg@alum.mit.edu; kristy@fractal.colorado.edu)

W. Klein, Department of Physics, Boston University, 590 Commonwealth Avenue, Room 255, Boston, MA 02215, USA. (klein@physics.bu.edu)

J. B. Rundle, Center for Computational Science and Engineering, University of California, Davis, One Shields Avenue, Davis, CA 95616, USA. (rundle@physics.ucdavis.edu)

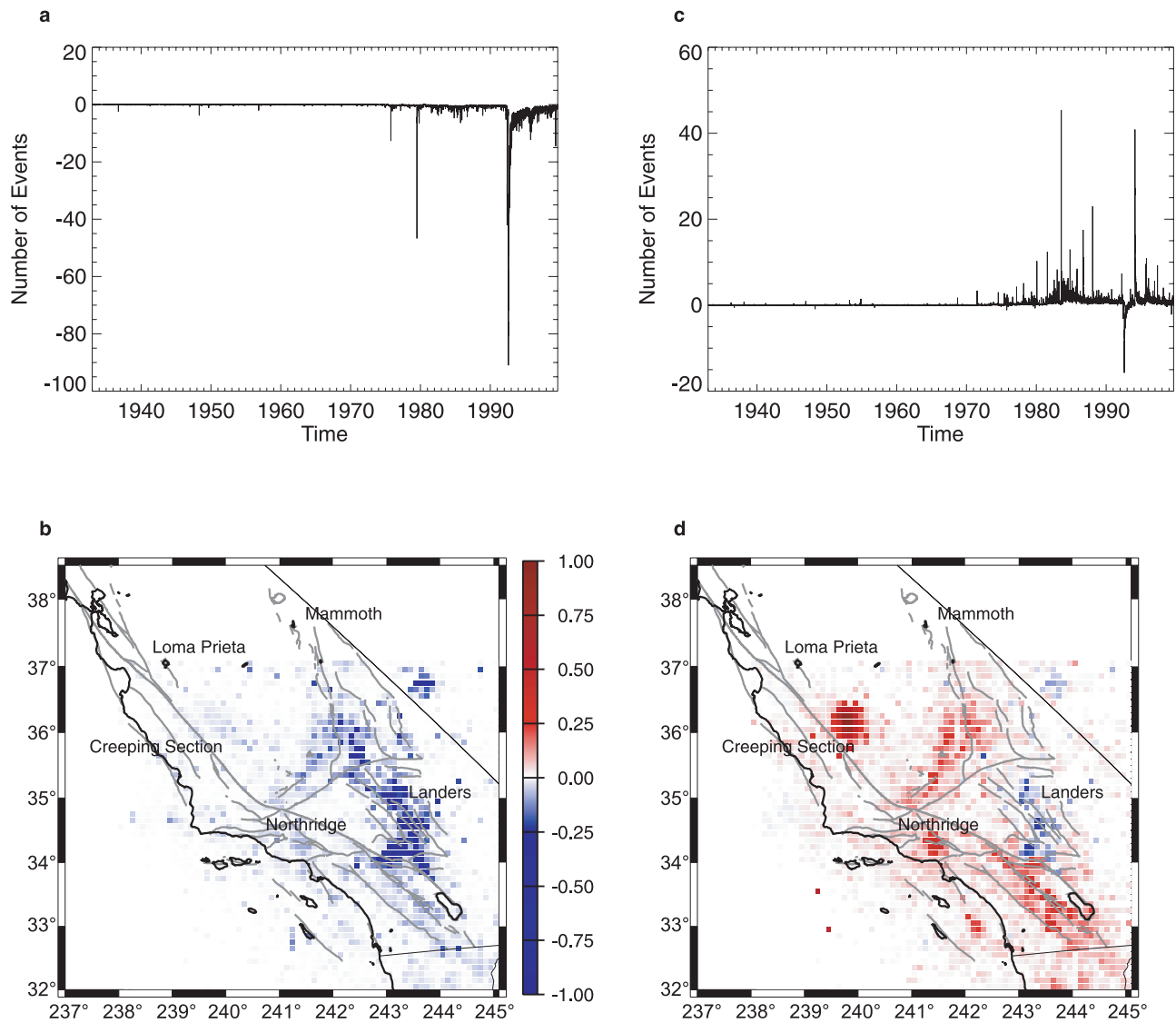


Figure 5. First two KLE modes for southern California seismicity, 1932–1999. (a) PC time series for first KLE mode, (b) first KLE mode, normalized to maximum, (c) PC time series for second KLE mode, and (d) second KLE mode, also normalized to the maximum.

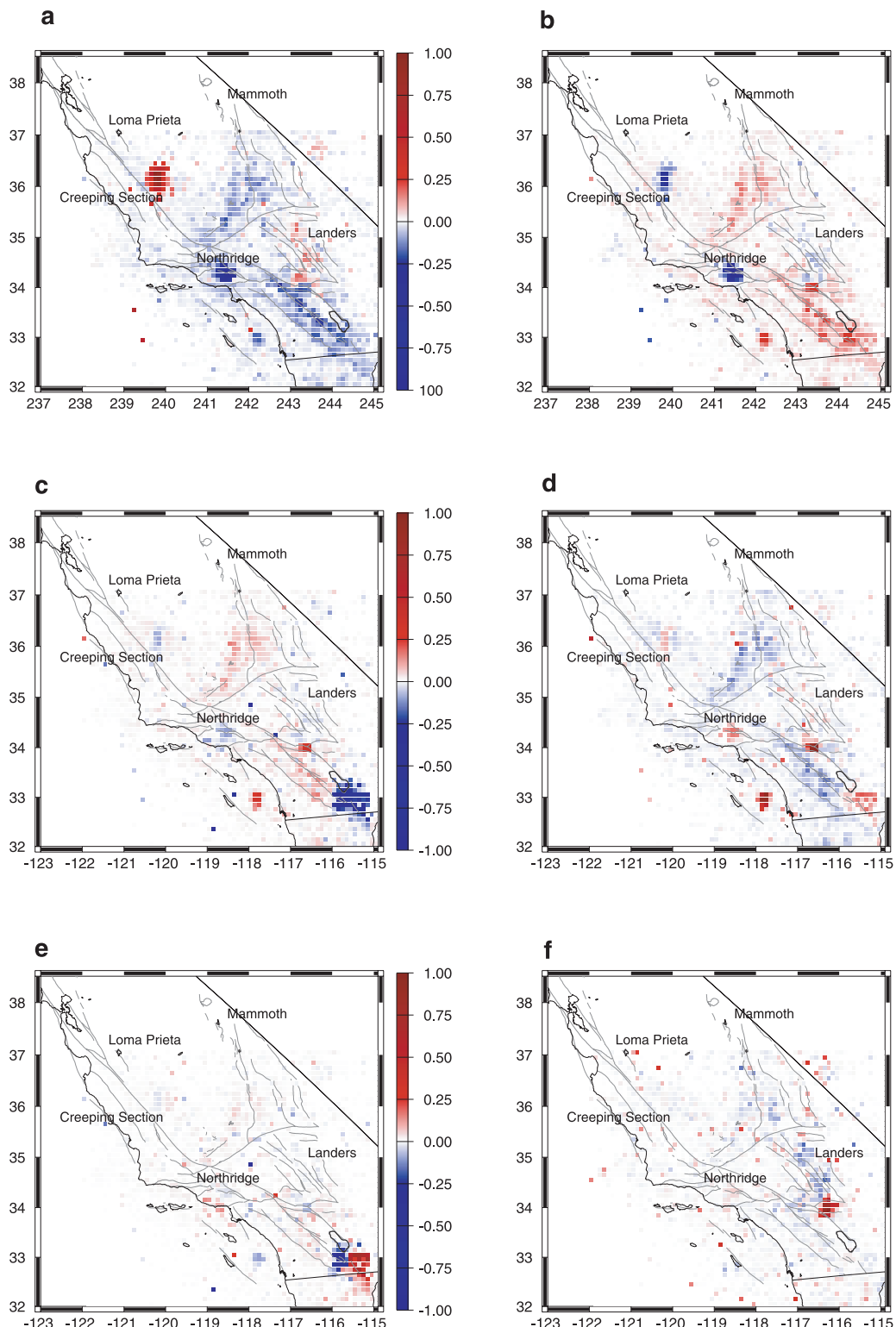


Figure 6. KLE modes three and four, six through nine, for southern California seismicity, 1932–1999, each normalized to the maximum. (a) Third KLE mode, normalized to maximum, (b) fourth KLE mode, (c) sixth KLE mode, (d) seventh KLE mode, (e) eighth KLE mode, and (f) ninth KLE mode.

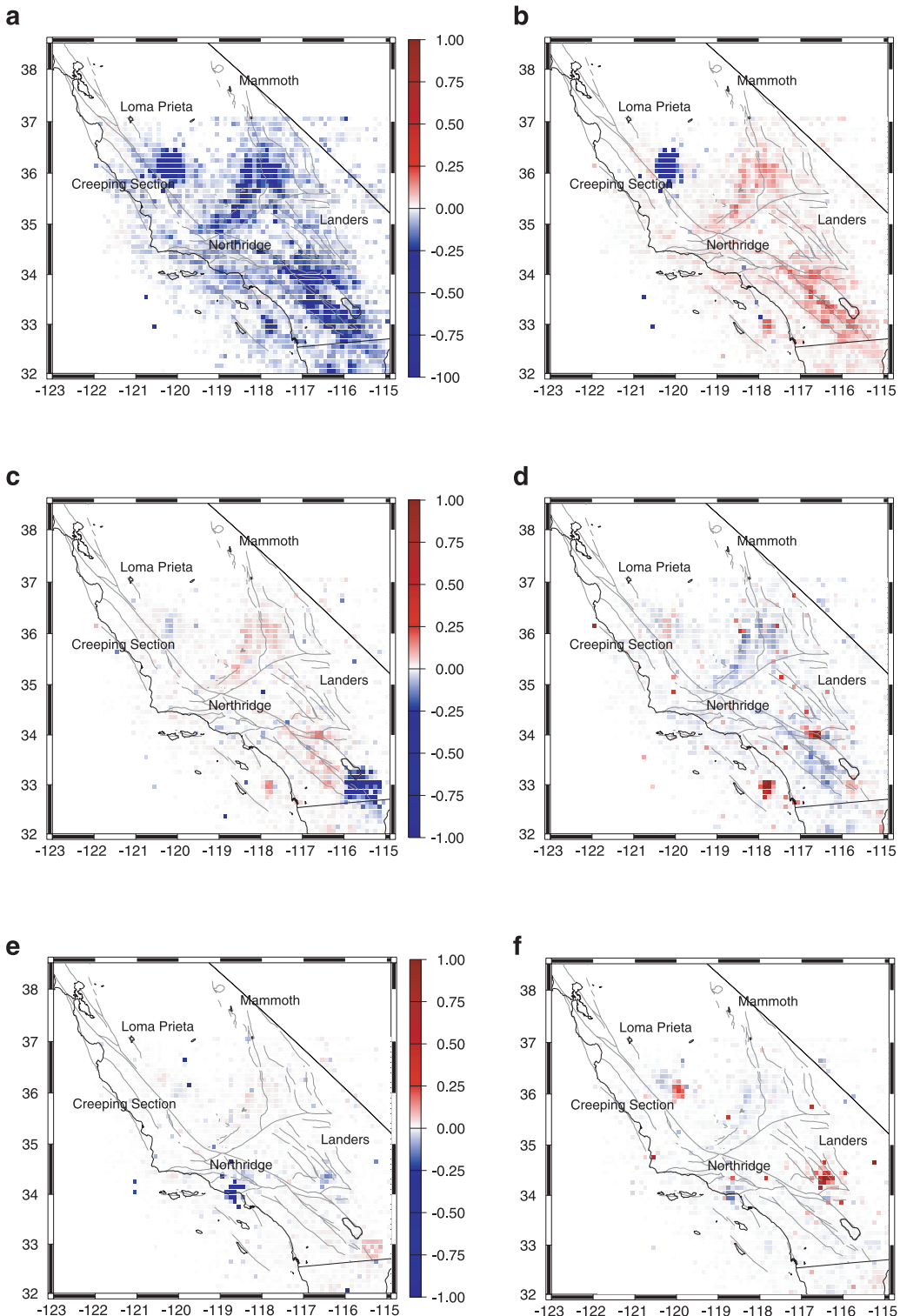


Figure 8. First two KLE modes, in addition to modes four, five, seven, and eight, for southern California seismicity, 1932–1991, normalized to the maximum. (a) First KLE mode, (b) second KLE mode, (c) fourth KLE mode, (d) fifth KLE mode, (e) seventh KLE mode, and (f) eighth KLE mode.

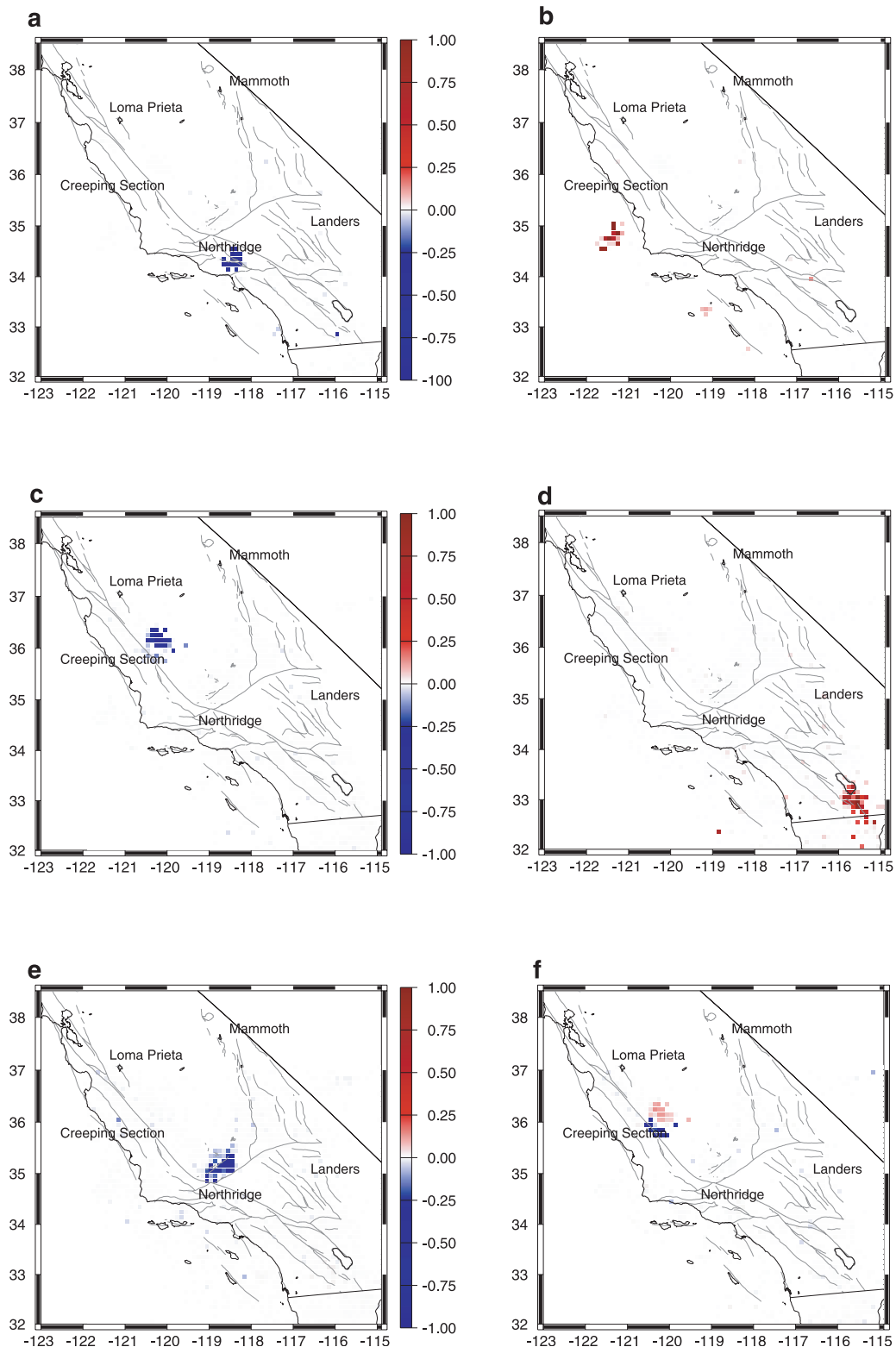


Figure 9. (a) First KLE mode, (b) second KLE mode, (c) third KLE mode, (d) fourth KLE mode, (e) seventh KLE mode, and (f) eleventh KLE mode for southern California seismicity, $M < 3.0$, 1932–1991, each normalized to its maximum.

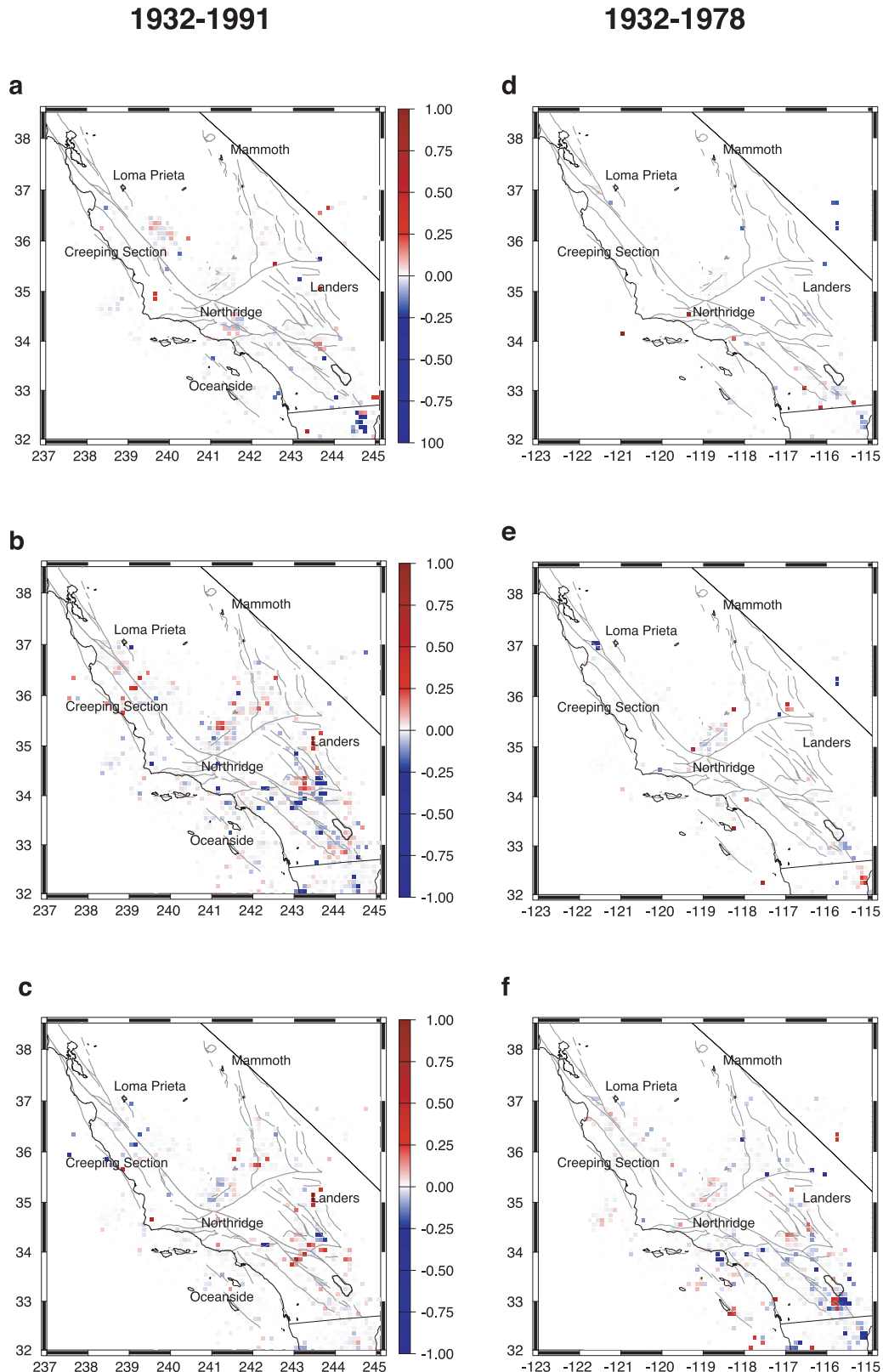


Figure 11. (a) KLE mode 49, (c) KLE mode 58, and (d) KLE mode 62 for southern California seismicity, $M > 3.0$, 1932–1991, each normalized to its maximum. For 1932–1978, (d) KLE mode, (e) KLE mode, and (f) KLE mode 62, southern California seismicity, $M > 3.0$, each normalized to its maximum.